# Probing the Functional Role of Ca 2+ in the Oxygen-Evolving Complex of Photosystem II by Metal Ion Inhibition †

**ARTICLE** *in* BIOCHEMISTRY · APRIL 2007

Impact Factor: 3.02 · DOI: 10.1021/bi062033i · Source: PubMed



**3 AUTHORS**, INCLUDING:

Cheng-I Lee
National Chung Cheng University
**18** PUBLICATIONS **235** CITATIONS

SEE PROFILE

K. V. Lakshmi
Rensselaer Polytechnic Institute
**78** PUBLICATIONS **2,409** CITATIONS

SEE PROFILE

# Probing the Functional Role of $Ca^{2+}$ in the Oxygen-Evolving Complex of Photosystem II by Metal Ion Inhibition†

Cheng-I Lee,§,# K. V. Lakshmi,‡ and Gary W. Brudvig*,§

*Department of Chemistry, Yale University, P.O. Box 208107, New Haven, Connecticut 06520-8107, and Department of Chemistry and Chemical Biology, Rensselaer Polytechnic Institute, Troy, New York 12180-3590*

*Received September 29, 2006; Revised Manuscript Received December 21, 2006*

ABSTRACT: Photosynthetic oxygen evolution in photosystem II (PSII) takes place in the oxygen-evolving complex (OEC) that is comprised of a tetranuclear manganese cluster ($Mn_4$), a redox-active tyrosine residue ($Y_Z$), and $Ca^{2+}$ and $Cl^-$ cofactors. The OEC is successively oxidized by the absorption of 4 quanta of light that results in the oxidation of water and the release of $O_2$. $Ca^{2+}$ is an essential cofactor in the water-oxidation reaction, as its depletion causes the loss of the oxygen-evolution activity in PSII. In recent X-ray crystal structures, $Ca^{2+}$ has been revealed to be associated with the $Mn_4$ cluster of PSII. Although several mechanisms have been proposed for the water-oxidation reaction of PSII, the role of $Ca^{2+}$ in oxygen evolution remains unclear. In this study, we probe the role of $Ca^{2+}$ in oxygen evolution by monitoring the $S_1$ to $S_2$ state transition in PSII membranes and PSII core complexes upon inhibition of oxygen evolution by $Dy^{3+}$, $Cu^{2+}$, and $Cd^{2+}$ ions. By using a cation-exchange procedure in which $Ca^{2+}$ is not removed prior to addition of the studied cations, we achieve a high degree of reversible inhibition of PSII membranes and PSII core complexes by $Dy^{3+}$, $Cu^{2+}$, and $Cd^{2+}$ ions. EPR spectroscopy is used to quantitate the number of bound $Dy^{3+}$ and $Cu^{2+}$ ions per PSII center and to determine the proximity of $Dy^{3+}$ to other paramagnetic centers in PSII. We observe, for the first time, the $S_2$ state multiline electron paramagnetic resonance (EPR) signal in $Dy^{3+}$- and $Cd^{2+}$-inhibited PSII and conclude that the $Ca^{2+}$ cofactor is not specifically required for the $S_1$ to $S_2$ state transition of PSII. This observation provides direct support for the proposal that $Ca^{2+}$ plays a structural role in the early S-state transitions, which can be fulfilled by other cations of similar ionic radius, and that the functional role of $Ca^{2+}$ to activate water in the O−O bond-forming reaction that occurs in the final step of the S state cycle can only be fulfilled by $Ca^{2+}$ and $Sr^{2+}$, which have similar Lewis acidities.

The photooxidation of water to dioxygen in plants, algae, and cyanobacteria is catalyzed by the oxygen-evolving complex (OEC)[1] of photosystem II (PSII). The photochemistry of PSII is initiated by photoinduced charge separation from a primary chlorophyll, $P_{680}$, to a pheophytin (Pheo) and subsequently to the membrane-bound quinone cofactors, $Q_A$ and $Q_B$, which results in stabilization of the charge-separated states. The OEC of PSII is comprised of a tetranuclear manganese cluster ($Mn_4$), a redox-active tyrosine residue ($Y_Z$), and calcium ion ($Ca^{2+}$) and chloride ion ($Cl^-$) cofactors (Figure 1). To further stabilize the charge-separated state, $P680^{\bullet+}$ is reduced by a tyrosine residue, $Y_Z$, in the OEC, which in turn is reduced by the $Mn_4$ cluster. During the oxygen-evolution reaction, the $Mn_4$ cluster is sequentially oxidized in four light-driven steps. The successive formation of the higher oxidation states of the $Mn_4$ cluster, called $S_n$ states ($n = 0-4$), leads to the oxidation of two water molecules and the release of one molecule of dioxygen (*1*, *2*).

$Ca^{2+}$ has been identified as an essential cofactor in the oxygen-evolution reaction, as the depletion of $Ca^{2+}$ ions from the OEC causes the loss of oxygen-evolving activity in PSII. The $Ca^{2+}$-binding sites in PSII have been previously studied by several methods (*3*−*6*). Although a varying number of $Ca^{2+}$-binding site(s) have been reported in the literature, it is generally accepted that one $Ca^{2+}$ ion per PSII center is required for oxygen evolution and that this $Ca^{2+}$ ion is tightly bound ($K_D \sim \mu M$) in the OEC. Besides the direct functional role of $Ca^{2+}$ ions in oxygen evolution, it has been suggested that a $Ca^{2+}$ site in the 33 kDa polypeptide on the donor side of PSII could regulate $H^+$ transfer pathways through the

† This work was supported by NIH Grant GM32715 and NSF Grant CHE-0215926 for purchase of the ELEXSYS E500 EPR spectrometer.

* Corresponding author. Phone: +1-203-432-5202. Fax: +1-203-432-6144. E-mail: gary.brudvig@yale.edu.

§ Yale University.

‡ Rensselaer Polytechnic Institute.

# Current Address: Medical Biotechnology Center, University of Maryland Biotechnology Institute, Baltimore, MD 21201.

[1] Abbreviations: bRC: bacterial reaction center; Chl: chlorophyll; DCBQ: 2,5-dichloro-*p*-benzoquinone; EDTA: ethylenediaminetetraacetic acid; EPR: electron paramagnetic resonance; EXAFS: extended X-ray absorption fine structure; FTIR: Fourier transform infrared; kDa: kilodalton; MES: 2-(*N*-morpholino)ethanesulfonic acid; $Mn_4$: tetranuclear manganese; OEC: oxygen-evolving complex; OGP: *n*-octyl-*β*-D-glucopyranoside; $P_{1/2}$: microwave power at half saturation; $P_{680}$: primary chlorophyll electron donor of PSII; Pheo: pheophytin; PPBQ: para-phenyl benzoquinone; PSII: photosystem II; $Q_A$: primary plastoquinone electron acceptor of PSII; $Q_B$: secondary plastoquinone electron acceptor of PSII; $S_n$ states: $S_0$ to $S_4$ oxidation states of the $Mn_4$ cluster; SDS−PAGE: sodium dodecyl sulfate−polyacrylamide gel electrophoresis; $Y_D$: redox-active tyrosine-160 residue of the D2 protein; $Y_Z$: redox-active tyrosine-161 residue of the D1 protein.

10.1021/bi062033i CCC: $37.00 
Published on Web 02/20/2007

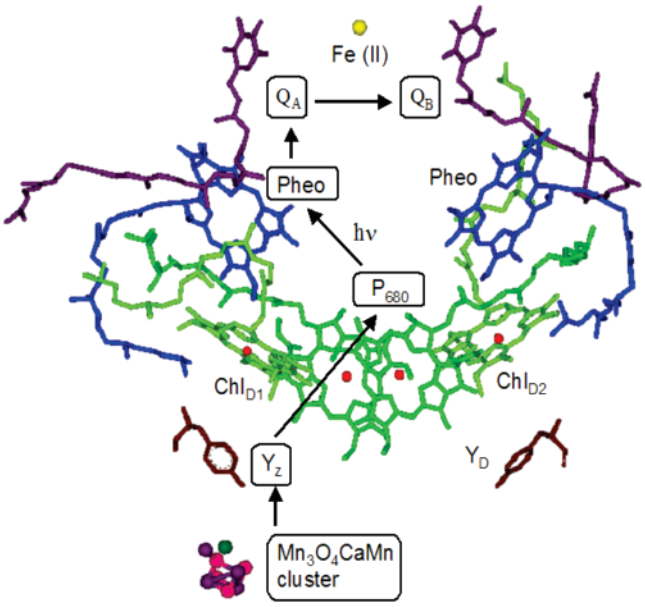


FIGURE 1: Relative locations of important redox components in PSII based on the 3.5 Å resolution crystal structure (PDB code: 1S5L) (*23*). Indicated with black arrows is the primary electron-transfer pathway of PSII.

water channel of the OEC (*7*, *8*) and a $Ca^{2+}$ site on the acceptor side of PSII could regulate proton-coupled electron-transfer pathways at the secondary quinone site of PSII (*9*). In addition, Shen, Ono, and co-workers have suggested the presence of additional $Ca^{2+}$ sites that could also indirectly influence $O_2$ evolution (*10*, *11*), and a weaker binding $Ca^{2+}$ site has been identified in the CP29 polypeptide of the light harvesting complex II (LHCII) (*12*) of PSII. However, in the absence of direct experimental evidence, the role(s) of these additional $Ca^{2+}$-binding site(s) in PSII are currently under debate.

$Sr^{2+}$ is the only cation that can functionally substitute for $Ca^{2+}$ in the OEC. The biosynthetic incorporation of $Sr^{2+}$ in the cyanobacterium *Thermosynechococcus elongatus* has recently been reported by Sugiura and co-workers (*13*). This study demonstrates that $Ca^{2+}$ can be biosynthetically replaced by $Sr^{2+}$ while retaining photosynthetic growth. Moreover in the thermophile, any $Sr^{2+}$ bound outside the OEC can be exchanged with $Ca^{2+}$ after isolating PSII, while the $Sr^{2+}$ ion bound in the OEC is nonexchangeable (*13*). The $Ca^{2+}$-binding properties of PSII from this thermophile differ from nonthermophilic PSII, for which $Ca^{2+}$ can be reversibly exchanged with di- and trivalent ions (*1*, *11*, *14*−*20*).

Previous results from extended X-ray absorption fine structure (EXAFS) measurements have indicated that the $Ca^{2+}$ ion in the OEC is located very close to the $Mn_4$ cluster with corresponding Mn−Ca distances of 3.3 Å (*17*−*19*) and 4.2 Å (*20*). More recently, the X-ray crystal structure of PSII has been solved at 3.8−3.0 Å resolution (*21*−*24*). The structure of the OEC cannot be discerned in atomic-level detail in these X-ray crystal structures. However, using the 3.5 Å resolution X-ray crystallography maps in conjunction with anomalous diffraction and molecular modeling, Barber, Iwata, and co-workers have identified a $Ca^{2+}$ ion as part of the OEC, which is modeled as a manganese-oxo cubane structure ($Mn_3CaO_4$) with a fourth manganese attached as a dangling atom (Figure 1). Additionally, Saenger, Zouni and co-workers solved the X-ray crystal structure of PSII at 3.0 Å resolution (*24*). The 3.0 Å resolution X-ray crystal structure identifies a $Mn_4Ca$ cluster, although the ligand assignment of the $Mn_4Ca$ cluster is different from the $Mn_3CaO_4$ cubane proposed by Barber, Iwata, and co-workers (*23*). The crystallographic results showing that calcium is part of the OEC emphasize the important role of a $Ca^{2+}$ ion in oxygen evolution.

Early proposals for the mechanism of oxygen evolution in PSII did not explain the role of $Ca^{2+}$ (*25*), which is known to be an essential cofactor for oxygen evolution. More recently, studies have suggested that $Ca^{2+}$ is directly involved in oxygen evolution (*26*−*29*). On the basis of density functional theory calculations, which showed that $Ca^{2+}$ might be directly bridged to the $Mn_4$ cluster by $\mu$-OH or $\mu$-O ligands, it has been suggested that $Ca^{2+}$ is required to form an oxygen radical in the $S_3$ state of the OEC (*27*). In a separate proposal, Pecoraro and co-workers have suggested that a terminal Mn(V)═O undergoes a nucleophilic attack by a $Ca^{2+}$-bound hydroxide ligand to form a Mn-bound hydroperoxide (*28*). Brudvig and co-workers have also proposed a mechanism in which a $Ca^{2+}$ ion plays a role as a weak Lewis acid beyond the $S_3$ state of the OEC whereby a $Ca^{2+}$-bound water reacts with a Mn(V)═O species to form the O−O bond through a nucleophilic attack (*26*).

In previous metal-ion inhibition studies, Brudvig and co-workers investigated the binding of mono-, di-, and trivalent cations to the $Ca^{2+}$-binding site in the OEC (*29*). These studies have suggested that the $Ca^{2+}$-binding site in the OEC of PSII is size-selective, similar to the binding of $Ca^{2+}$ ions in EF-hand proteins (*29*). Among the di- and trivalent cations that have been used to replace $Ca^{2+}$ in PSII, $Sr^{2+}$ is the only cation that maintains the $O_2$-evolving activity of PSII. This may be because $Sr^{2+}$ has a similar Lewis acidity to $Ca^{2+}$ (*29*, *30*). $Sr^{2+}$ ion substitution has been shown to alter the $S_2$ state multiline EPR signal (*31*). It has previously been demonstrated that the depletion of $Ca^{2+}$ ions in PSII does not inhibit the formation of the $S_2$ state (*32*, *33*). This result suggests that $Ca^{2+}$ may play a functional role beyond the $S_2$ state of the $Mn_4$ cluster in the OEC. It is thought that the incubation of PSII with $Dy^{3+}$ (*34*, *35*), $La^{3+}$ (*35*), and $Cd^{2+}$ (*11*, *36*, *37*) leads to loss of the ability to advance to the $S_2$ state in PSII as the $S_2$ state EPR signal has not been observed in these samples. The failure to observe the $S_2$ state EPR signal in these samples is inconsistent with the previous proposal that $Ca^{2+}$ is not required in the $S_1$ to $S_2$ state transition, but this could be ascribed to several other possibilities. First, the $Dy^{3+}$, $La^{3+}$, and $Cd^{2+}$ treatments may disrupt the calcium site or even disassemble the $Mn_4$ cluster and thus interrupt the $S_1$ to $S_2$ state transition. Second, the substitution of $Ca^{2+}$ by $Dy^{3+}$, $La^{3+}$, and $Cd^{2+}$ may decrease the rate of electron transfer from the $Mn_4$ cluster such that the conditions necessary to monitor the $Dy^{3+}$-, $La^{3+}$-, and $Cd^{2+}$-treated PSII samples are different from the conditions previously used for untreated PSII samples.

In this study, we examine the inhibition of oxygen evolution by divalent and trivalent metal ions in both BBY-type PSII-enriched membranes and PSII core complexes. By using a cation-exchange procedure in which $Ca^{2+}$ is not removed prior to addition of the studied cations (*29*), we achieve a high degree of reversible inhibition of PSII membranes and PSII core complexes by $Dy^{3+}$, $Cu^{2+}$, and

$Cd^{2+}$ ions. A single tightly bound $Dy^{3+}$ gives large and reversible inhibition of $O_2$ evolution and a significant enhancement of the $P_{1/2}$ of the $S_2$ state multiline signal, showing that this $Dy^{3+}$ binds close to $Mn_4$ cluster. We observe, for the first time, that both $Dy^{3+}$- and $Cd^{2+}$-inhibited PSII core complexes advance to the $S_2$ state and conclude that the $Ca^{2+}$ cofactor is not specifically required for the $S_1$ to $S_2$ state transition of PSII.

## MATERIALS AND METHODS

*BBY and Core Preparations of PSII.* BBY-type PSII-enriched membranes were isolated from market spinach according to the procedure of Berthold et al. (*38*) with the modifications of Beck et al. (*39*). The PSII samples were stored until use at 77 K in buffer containing 20 mM MES (pH 6.0), 15 mM NaCl, and 30% (v/v) ethylene glycol. PSII core complexes were prepared by the method of Ghanotakis et al. (*40*) with modifications. The BBY-type PSII-enriched membranes were washed three times with wash buffer (50 mM MES (pH 6), 10 mM NaCl, and 0.4 M sucrose) and resuspended in wash buffer to 2.5 mg of Chl/mL. The crucial step in the preparation of PSII core complexes is the dropwise addition of an equal volume of solubilization buffer (50 mM MES (pH 6), 5 mM $CaCl_2$, 10 mM NaCl, 1 M sucrose, and 70 mM *n*-octyl-$\beta$-D-glucopyranoside (OGP)), which dilutes the samples to 1.25 mg of Chl/mL. The 35 mM OGP extraction lasted for 10 min. Subsequently, the concentration of OGP was diluted from 35 mM to 15 mM by the addition of dilution buffer (50 mM MES (pH 6), 5 mM $CaCl_2$, 10 mM NaCl, 1 M sucrose), and the mixture was incubated at 0 °C for 5 min. PSII core complexes were soluble after a 20 min centrifuge spin at 34000*g*, while LHCII complexes precipitated as a pellet. The suspension was subsequently dialyzed against buffer containing 50 mM MES (pH 6), 10 mM NaCl, 5 mM $CaCl_2$, and 30% (v/v) ethylene glycol. Typically, repeated 30 min dialyses (2−3 times) will cause the aggregation of PSII core complexes. Two-fold dilution of the core complexes with dialysis buffer was followed by a centrifuge spin at 34000*g* for 30 min, which sediments the PSII core complexes. Collection of the PSII core complexes was achieved by resuspending PSII with a minimum amount of dialysis buffer. Complete removal of the light harvesting complexes and the 17 and 23 kDa extrinsic proteins was confirmed by SDS−PAGE using a 12% (w/v) acrylamide resolving gel (data not shown).

*$O_2$-Evolution Activity Measurements.* $O_2$-evolving activity measurements of PSII samples were performed with a Clark-type electrode at 25 °C (*39*). An Oriel 1000 W tungsten lamp, fitted with a liquid filter (filled with distilled water), a 610 nm cutoff filter (LP 610), and a heat filter, was used to initiate the photochemistry. 250 $\mu$M DCBQ and 1 mM $K_3Fe(CN)_6$ were added as an artificial electron acceptor and oxidant, respectively. Typically, $O_2$-evolution rates of 400−600 and 1000−1500 $\mu$mol of $O_2$ (mg of Chl)$^{-1}$ h$^{-1}$ were observed for PSII membranes and PSII core complexes, respectively, in buffer containing 20 mM MES (pH 6.0), 15 mM NaCl, and 20 mM $CaCl_2$.

*Time Course of Cation-Exchange Equilibrium.* The time course of the exchange of $Ca^{2+}$ in PSII with divalent and trivalent cations was investigated by monitoring the inhibition of $O_2$-evolving activity of PSII during the course of the cation treatments. The completion of the cation exchange is determined to be the point at which the $O_2$-evolving activity of the PSII sample no longer decreases. The equilibrium time of cation exchange in PSII membranes and in PSII core complexes are compared in this study.

*Inhibition of Oxygen Evolution by $Dy^{3+}$ Ions.* The inhibition of oxygen evolution by $Dy^{3+}$ ions in BBY-type PSII membranes has been conducted under various conditions. The $Dy^{3+}$-inhibited PSII samples, Dy1−Dy3, were prepared by a 4-h incubation of PSII membranes in the presence of 20 mM MES (pH 6), 15 mM NaCl, and 20 mM $DyCl_3$ (Dy1), subsequent incubation with 50 mM MES (pH 6), 15 mM OGP, 5 mM $CaCl_2$, 0.4 M NaCl, and 1 M sucrose (Dy2), and further treatment with 1 mM EDTA (Dy3). PSII samples, Dy4 and Dy5, were both prepared directly from PSII membranes by 15 min incubation with 50 mM MES (pH 6), 15 mM OGP, 0.4 M NaCl, 1 M sucrose, and 0.5 mM $DyCl_3$ (Dy4) or 0.1 mM $DyCl_3$ (Dy5), respectively. PSII samples, Dy6 and Dy7, were obtained by a method similar to the preparation of Dy5 except that the buffer was pretreated with Chelex 100 for one and two times, respectively, to remove residual $Ca^{2+}$ ions. All of the $Dy^{3+}$-inhibited PSII samples (Dy1−Dy7, respectively) were washed or dialyzed against $Dy^{3+}$-free buffer to remove excess unbound $Dy^{3+}$ ions in solution. The inhibition of oxygen evolution by $Dy^{3+}$ was confirmed by the significant decrease of the oxygen-evolving activity upon treatment with $Dy^{3+}$ ions. Further, the reversibility of the $Dy^{3+}$ treatment was examined by monitoring the oxygen-evolving activity after reconstitution of PSII with 20 mM $CaCl_2$. The inhibition of oxygen evolution by $Dy^{3+}$ in PSII core complexes was examined in Chelex 100 treated buffer (20 mM MES (pH 6) and 15 mM NaCl) by the addition of 0.001 to 0.3 mM $DyCl_3$ followed by a 5 min incubation period. Similarly, the $Dy^{3+}$ inhibition and $Ca^{2+}$ reconstitution were examined by conducting oxygen-evolving activity assays after the sample treatments. The correlation of the EPR signal intensity of $DyCl_3$ EPR spin standards was established as shown in Figure 2. The concentration of $Dy^{3+}$ ions in each of the $Dy^{3+}$-inhibited PSII samples was quantitated by comparison of the EPR signal intensity of $Dy^{3+}$ in PSII with that of the $DyCl_3$ EPR spin standards. The number of metal ions per PSII center was estimated based on the calculation that one BBY-type PSII center has 200 chlorophylls and one PSII core complex has 38 chlorophylls.

*Inhibition of Oxygen Evolution by $Cu^{2+}$ and $Cd^{2+}$ Ions.* The inhibition of oxygen evolution by $Cu^{2+}$ was achieved by methods similar to those used for $Dy^{3+}$ inhibition of PSII. The PSII samples, Cu1, Cu2, and Cu3, were prepared from BBY-type PSII membranes. PSII samples, Cu1 and Cu2, were incubated at pH 6 with $CuCl_2$ (1.5 and 0.5 mM for Cu1 and Cu2, respectively), 15 mM OGP, 0.4 M NaCl, 1 M sucrose, and 50 mM MES for 15 min, followed by 3 washes with an excess of solution containing 20 mM MES, 15 mM NaCl, and 0.1 mM EDTA (pH 6). For preparation of the PSII sample, Cu3, all of the buffers were pretreated with Chelex 100 twice; otherwise, the procedure was the same as that used to prepare the PSII sample, Cu2. The $Cu^{2+}$ inhibition of PSII core complexes was investigated over the range from 0.001 to 2 mM $CuCl_2$ obtained by addition of a stock solution to Chelex 100 treated buffer (20 mM MES (pH 6) and 15 mM NaCl). After incubation with $CuCl_2$-

containing buffers, all the samples were washed with $Cu^{2+}$-free buffers several times to remove unbound $Cu^{2+}$ ions. The number of $Cu^{2+}$ ions was determined by comparison of the EPR signal intensity of the $g = 2.6$ to $g = 1.8$ signals in $Cu^{2+}$-inhibited PSII samples with those of $Cu^{2+}$-EDTA EPR spin standards.

The inhibition of oxygen evolution by $Cd^{2+}$ was conducted only in PSII core complexes. The inhibition was achieved by incubating the PSII core complexes in buffers at pH 6 containing 20 mM MES and 15 mM NaCl, and $CdCl_2$ at concentrations ranging from 0.5 to 6 mM.

*EPR Measurements. (a) EPR Spectroscopy of the Light-Induced Signals of PSII.* All the PSII samples were dark adapted after the addition of 1 mM $K_3Fe(CN)_6$ and 0.5 mM PPBQ to keep the electron acceptors in PSII completely oxidized prior to conducting EPR measurements. The $S_2$ state multiline EPR signal was obtained by 1−5 min illumination at 200 K (in a dry ice and acetone bath) followed by rapid freezing of the PSII samples at 77 K. The dark-stable $Y_D^{\bullet}$ EPR signal was induced by illumination at 0 °C for 2 to 5 min. All the EPR scans were acquired on a Varian E-line EPR spectrometer equipped with a $TE_{102}$ cavity or a Brüker ELEXYS E500 EPR spectrometer equipped with a SHQ resonator and an Oxford ESR-900 helium-flow cryostat. The $S_2$ state multiline EPR signal was recorded at 6 K with the following instrumental parameters: microwave frequency = 9.28 GHz (Varian) or 9.38 GHz (Brüker), modulation frequency = 100 kHz, modulation amplitude = 20 G. The experimental parameters for the observation of the $Y_D^{\bullet}$ EPR signal were as follows: temperature = 30 K, microwave frequency = 9.28 GHz (Varian) or 9.38 GHz (Brüker), modulation frequency = 100 kHz, modulation amplitude = 2 G. The microwave power was varied as indicated in the figure captions of the EPR spectra.

*(b) Simulation of EPR Progressive Power Saturation Data.* The EPR progressive power saturation curves were simulated using the equation:

$$A = \frac{K\sqrt{P}}{(1 + P/P_{1/2})^{b/2}} \quad (1)$$

where $A$ is the EPR signal amplitude, $K$ is a constant, $P$ is the microwave power, $P_{1/2}$ is the microwave power at half-saturation, and $b$ is the inhomogeneity parameter. For a first-derivative EPR spectrum, $b = 1$ in the inhomogeneous limit and $b = 3$ in the homogeneous limit. In this work, the inhomogeneous limit was used, and the value of $b$ was set to 1. The progressive power-saturation curves were simulated using Origin 6.0 (Microcal Software, Inc.).

*(c) $Dy^{3+}$ EPR Signals.* The EPR signal of $Dy^{3+}$ has a broad peak located at $g \sim 16$ (Figure 2). The EPR signal of $Dy^{3+}$ ions in the $DyCl_3$ EPR spin standards and $Dy^{3+}$ ions in PSII are compared for the quantitation of bound $Dy^{3+}$ in PSII. The instrumental parameters used to observe the $Dy^{3+}$ EPR signals were as follows: microwave frequency = 9.28 GHz, modulation frequency = 100 kHz, modulation amplitude = 20 G, microwave power = 5 mW and the EPR spectra were recorded at 6 K on a Varian EPR spectrometer.

*(d) $Cu^{2+}$ EPR Signals.* The EPR signal of $Cu^{2+}$ consists of hyperfine splittings between $g = 1.8$ and $g = 2.6$ that are sensitive to the binding environment of the $Cu^{2+}$ ions. The instrumental parameters for observation of the $Cu^{2+}$ ions are same as those used for recording $Dy^{3+}$ EPR signals. The quantitation of bound $Cu^{2+}$ ions in PSII was achieved by double integration of the $Cu^{2+}$ hyperfine peaks using the method of Aasa and Vänngård (*41*).

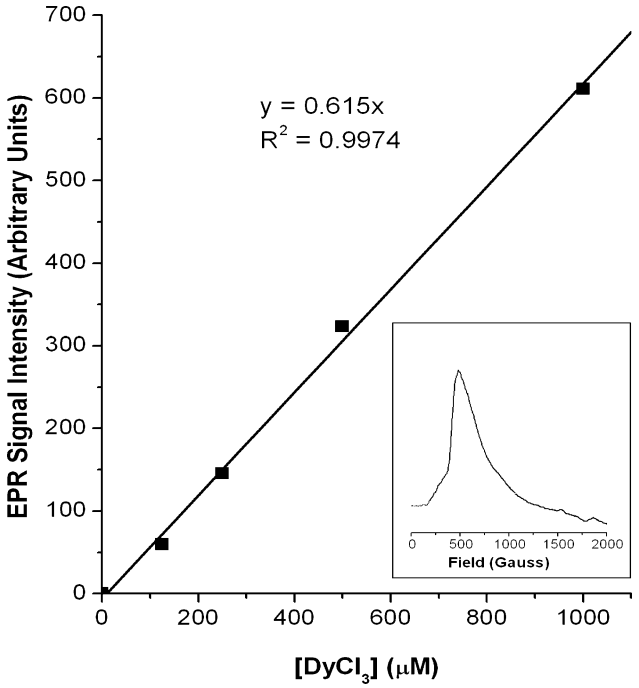


FIGURE 2: Correlation of the EPR signal intensity with the concentration of $DyCl_3$ spin standards. The $Dy^{3+}$ EPR signal is shown in the inset.

## RESULTS

*Inhibition by $Dy^{3+}$ Ions. (a) Oxygen-Evolution Inhibition Data.* In the present study, the inhibition of oxygen evolution of PSII by $Dy^{3+}$ has been conducted in both PSII membranes and PSII core complexes. The inhibition of oxygen evolution by $Dy^{3+}$ in PSII membranes requires a 4 h incubation period to achieve equilibrium, whereas the inhibition of oxygen evolution with $Dy^{3+}$ in PSII core complexes is rapid and complete within few minutes (Figure 3). Several conditions have been examined for the preparation of $Dy^{3+}$-inhibited PSII membranes. Table 1 summarizes the characterization of $Dy^{3+}$-inhibited PSII membranes and $Dy^{3+}$-inhibited PSII core complexes. Most notably, the addition of 20 mM $CaCl_2$ to the $Dy^{3+}$-treated PSII samples (Dy4−Dy7) restores 60−71% of the original oxygen-evolving activity of untreated PSII.

The incubation of PSII membranes with excess $DyCl_3$ (sample Dy1) for 4 h achieves complete $Dy^{3+}$ inhibition, and the number of bound $Dy^{3+}$/PSII center is determined to be 24 (Table 1). Further treatment with EDTA lowers the number of bound $Dy^{3+}$/PSII to 19 and 6 for samples Dy2 and Dy3, respectively. Incubation of PSII membranes with lower concentrations of $DyCl_3$ gives 2 to 6 $Dy^{3+}$/PSII as characterized in samples Dy4−Dy7. As shown in Figure 4 and Table 1, the incubation of PSII core complexes with 0.3 mM $DyCl_3$ results in significant inhibition (93%) of $O_2$-evolving activity. It is determined that there is 1 bound $Dy^{3+}$/PSII present in this sample and there is high reversibility of inhibition (∼62%) upon reconstitution with $Ca^{2+}$. In samples

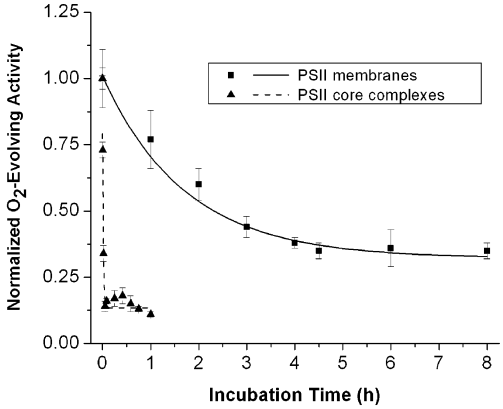


FIGURE 3: The time course of the exchange of $Ca^{2+}$ with $Dy^{3+}$ in BBY-type PSII membranes and PSII core complexes. Inhibition of oxygen evolution is achieved by the addition and incubation of $Dy^{3+}$ with PSII membranes in buffer containing 20 mM MES (pH 6), 15 mM NaCl, 5 mM $DyCl_3$, and 5 mM $CaCl_2$ and with PSII core complexes in buffer containing 20 mM MES (pH 6), 15 mM NaCl, and 5 mM $DyCl_3$. The curve fits of the experimental data indicate that equilibrium is reached in 4 h with the $Dy^{3+}$ incubation of PSII membranes and ~3 min with the $Dy^{3+}$ incubation of PSII core complexes.

Table 1: Summary of the Characterization of $Dy^{3+}$-Inhibited PSII Samples[a]

| $Dy^{3+}$-inhibited sample | % activity after $Dy^{3+}$-inhibition | $Dy^{3+}$/PSII | % activity after $Ca^{2+}$-reconsitiution |
|---|---|---|---|
| Dy1[b] | 0 | 24 | 0 |
| Dy2[b] | 0 | 19 | 0 |
| Dy3[b] | 0 | 6 | 0 |
| Dy4[b] | 20 ± 1[c] | 6 | 65 ± 3[c] |
| Dy5[b] | 45 ± 2[d] | 2 | 60 ± 5[d] |
| Dy6[b] | 14 ± 0[e] | 3 | 71 ± 2[e] |
| Dy7[b] | 9 ± 3[f] | 2 | 70 ± 2[f] |
| $Dy^{3+}$-PSII core complex | 7 ± 1[g] | 1 | 62 ± 5[g] |

[a] See sample preparation section for details. [b] Prepared from BBY-type PSII membranes: samples Dy1−Dy3 were prepared from incubation with 20 mM $DyCl_3$ (Dy1), a subsequent OGP-treatment (Dy2) and a further EDTA-treatment (Dy3); samples Dy4 and Dy5 were prepared from incubation with OGP, NaCl, EDTA and 0.5 or 0.1 mM $DyCl_3$, respectively; samples Dy6 and Dy7 were prepared with the same method of Dy5, but the buffer was pretreated with Chelex 100 once or twice, respectively. [c] Relative to activity of untreated PSII membranes at 630 $\mu$mol of $O_2$ (mg of Chl)$^{-1}$ h$^{-1}$. [d] Relative to activity of untreated PSII membranes at 647 $\mu$mol of $O_2$ (mg of Chl)$^{-1}$ h$^{-1}$. [e] Relative to activity of untreated PSII membranes at 460 $\mu$mol of $O_2$ (mg of Chl)$^{-1}$ h$^{-1}$. [f] Relative to activity of untreated PSII membranes at 432 $\mu$mol of $O_2$ (mg of Chl)$^{-1}$ h$^{-1}$. [g] Relative to activity of untreated PSII core complexes at 1228 $\mu$mol of $O_2$ (mg of Chl)$^{-1}$ h$^{-1}$.

Dy1−3, the $O_2$-evolving activity is inhibited completely and cannot be recovered by reconstitution with $CaCl_2$. However, $Dy^{3+}$ inhibition in samples Dy4−7 is reversible. Reconstitution with $Ca^{2+}$ restores >60% of the original $O_2$-evolving activity, as shown in Table 1. Similarly, the incubation of PSII core complexes with $CuCl_2$ and $CdCl_2$ was investigated (Figure 4).

*(b) EPR Spectroscopic Properties of $Dy^{3+}$-Inhibited PSII Core Complexes*. Shown in Figure 5 is a comparison of the light-induced $S_2$ state multiline EPR signal in (a) untreated PSII core complexes and (b) $Dy^{3+}$-inhibited PSII core complexes with a single $Dy^{3+}$ per PSII. After illumination of the $Dy^{3+}$-inhibited PSII core complexes at 200 K for 2 min, the $S_2$ state multiline and $Q_A^-$ EPR signals are observed at $g \sim 2$ and $g \sim 1.86$, respectively. The $S_2$ state multiline EPR signal in $Dy^{3+}$-inhibited PSII core complexes is very

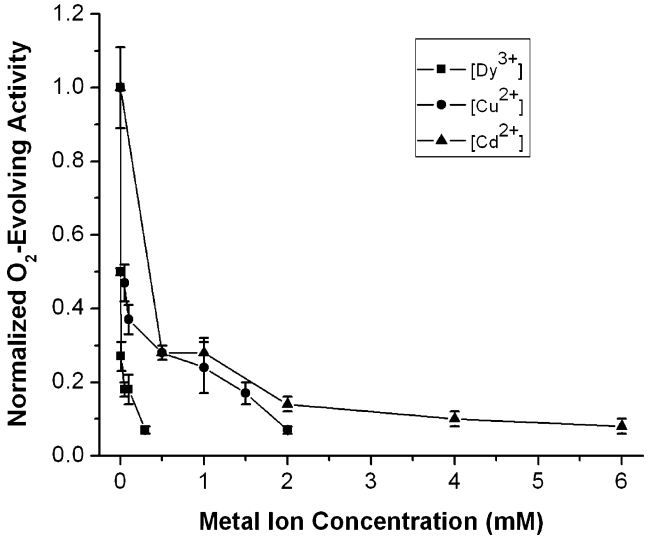


FIGURE 4: $Dy^{3+}$, $Cu^{2+}$, and $Cd^{2+}$ inhibition of PSII core complexes. The oxygen-evolving activity of the inhibited PSII samples was normalized to the activity of untreated PSII at 1228 $\mu$mol of $O_2$ (mg of Chl)$^{-1}$ h$^{-1}$. See text for sample preparation.

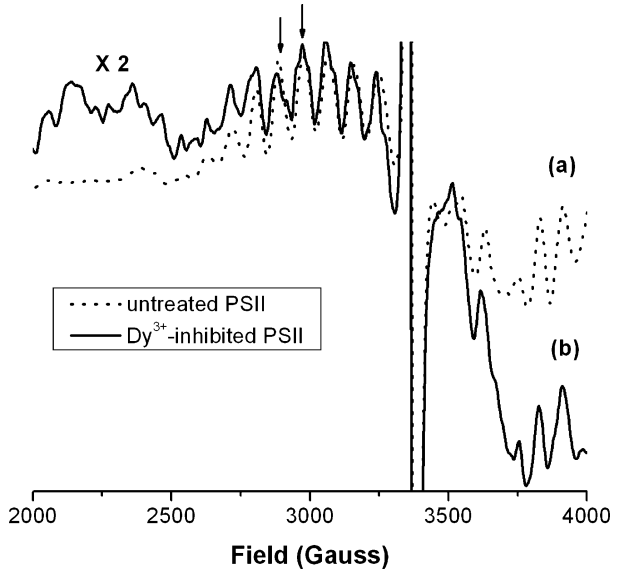


FIGURE 5: The $S_2$ state multiline EPR signal obtained from light-minus-dark spectra after illumination for 2 min at 200 K of (a) untreated PSII core complexes and (b) $Dy^{3+}$-inhibited PSII core complexes with 1 $Dy^{3+}$ bound per PSII. The EPR spectra were acquired with 1 and 10 mW on a Brüker EPR spectrometer for untreated and $Dy^{3+}$-inhibited PSII core complexes, respectively. The detection powers are close to the $P_{1/2}$ values of 0.92 and 9.9 mW for untreated and $Dy^{3+}$-inhibited PSII core complexes, respectively. The arrows indicate the $^{55}$Mn hyperfine peaks associated with the $S_2$ state multiline signal that were used for quantitation of the EPR signal intensity.

similar to the $S_2$ state multiline EPR signal in untreated PSII core complexes. However, the hyperfine peaks of the $S_2$ state multiline EPR signal in $Dy^{3+}$-inhibited PSII cores are slightly broader, and additional weak peaks are observed in the $g \sim 3$ region of the EPR spectrum. The yield of the $S_2$ state multiline EPR signal in $Dy^{3+}$-inhibited PSII core complexes and untreated PSII core complexes was investigated as a function of the illumination time at 200 K for (a) 1 min, (b) 2 min, (c) 3 min, (d) 4 min, and (e) 5 min (data not shown). It is observed that the spectral intensity of the $S_2$ state multiline EPR signal in untreated PSII core complexes and

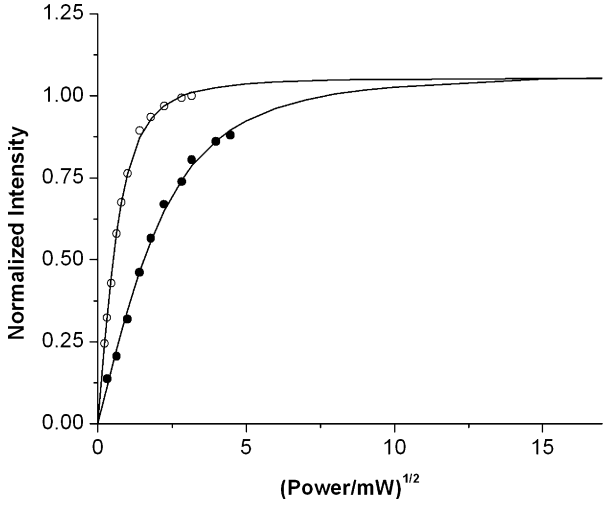


FIGURE 6: Progressive power saturation of the $S_2$ state multiline signal in untreated PSII core complexes (open circles) and $Dy^{3+}$-inhibited PSII core complexes (filled circles) after illumination at 200 K for 2 min. The $P_{1/2}$ is determined to be 0.92 mW ($R^2$ = 0.9988) and 9.9 mW ($R^2$ = 0.9876) for untreated PSII and $Dy^{3+}$-inhibited PSII core complexes, respectively. The spectra were collected on a Brüker EPR spectrometer.

$Dy^{3+}$-inhibited PSII core complexes remains unchanged with the increase in illumination time of the samples. The average yield of the $S_2$ state multiline EPR signal collected after 1−5 min illumination in $Dy^{3+}$-inhibited PSII core complexes is 24% of the average yield of the $S_2$ state multiline EPR signal in untreated PSII core complexes when the EPR signal intensity under non-saturating conditions is compared and corrections are made for sample concentration and microwave power.

*(c) Progressive Power Saturation of EPR Signals in $Dy^{3+}$-Inhibited PSII.* Figure 6 shows the progressive power saturation curves of the $S_2$ state multiline EPR signal in untreated PSII and $Dy^{3+}$-inhibited PSII core complexes. According to eq (1), the $P_{1/2}$ of the $S_2$ state multiline EPR signal in untreated PSII and $Dy^{3+}$-inhibited PSII core complexes is determined to be 0.92 and 9.9 mW, respectively. The power saturation of the $Y_D^\bullet$ EPR signal is investigated in untreated PSII, $Dy^{3+}$-inhibited PSII membranes (samples Dy1, Dy4, and Dy7) and $Dy^{3+}$-inhibited PSII core complexes as shown in Figure 7 a,b and Table 2. The intensity of the $Y_D^\bullet$ EPR signal is determined at the magnetic field position indicated by an arrow in the insets of Figure 7 a,b. The inhibition of oxygen evolution by $Dy^{3+}$ in PSII membranes with 2, 6, and 24 $Dy^{3+}$/PSII enhances the $P_{1/2}$ of $Y_D^\bullet$ from 0.27 mW to 0.5, 1.2, and 3.5 mW, respectively (measured on a Varian EPR spectrometer). In PSII core complexes, the inhibition of oxygen evolution by $Dy^{3+}$ enhances the $P_{1/2}$ of $Y_D^\bullet$ from 0.034 to 0.066 mW (measured on a Brüker EPR spectrometer). As different resonators are used on the Varian and Brüker EPR spectrometers, a normalization factor, determined by the ratio of the $P_{1/2}$ values of the $S_2$ state multiline EPR signal in untreated PSII membranes on the two spectrometers, was applied to the power saturation data. The raw and normalized $P_{1/2}$ values of $Y_D^\bullet$ are listed in Table 2.

*Inhibition by $Cu^{2+}$ Ions. (a) Oxygen-Evolution Inhibition Data.* The inhibition of oxygen evolution by $Cu^{2+}$ has been conducted in both BBY-type PSII membranes and PSII core

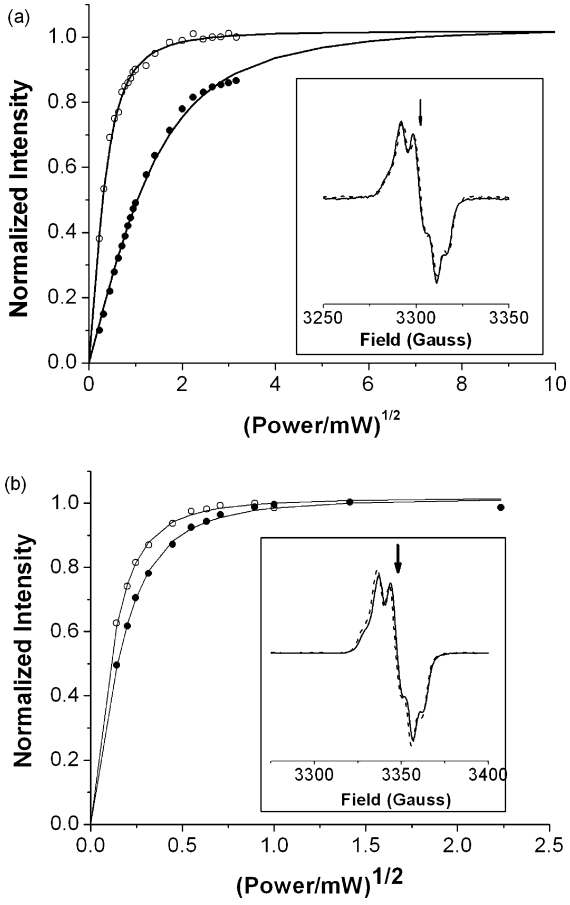


FIGURE 7: (a) Power saturation of the $Y_D^\bullet$ EPR signal in excess $Dy^{3+}$-inhibited PSII membranes (sample Dy1, filled circles) and untreated PSII membranes (open circles) at 30 K, measured on a Varian EPR spectrometer. The data yield $P_{1/2}$ of 3.5 mW ($R^2$ = 0.9967) and $P_{1/2}$ of 0.27 mW ($R^2$ = 0.9944) for $Dy^{3+}$-inhibited PSII membranes and untreated PSII membranes, respectively. The inset shows the $Y_D^\bullet$ EPR signal in $Dy^{3+}$-inhibited PSII membranes (sample Dy1, solid line) and untreated PSII membranes (dashed line) recorded at a microwave power of 0.3 mW. The arrow indicates the hyperfine peak of $Y_D^\bullet$ EPR signal that was used for quantitation. (b) Progressive power saturation of the $Y_D^\bullet$ signal in $Dy^{3+}$-inhibited PSII core complexes with 1 $Dy^{3+}$ per PSII (filled circles) and untreated PSII core complexes (open circles) at 30 K, measured on a Brüker EPR spectrometer. The data yield $P_{1/2}$ of 0.066 mW ($R^2$ = 0.9964) and $P_{1/2}$ of 0.034 mW ($R^2$ = 0.9954) for $Dy^{3+}$-inhibited PSII membranes and untreated PSII membranes, respectively. The inset shows the $Y_D^\bullet$ signal in $Dy^{3+}$-inhibited PSII core complexes (solid line) and untreated PSII core complexes (dashed line) recorded at a microwave power of 0.04 mW. The arrow indicates the hyperfine peak of the $Y_D^\bullet$ EPR signal that was used for quantitation.

complexes. Incubation of PSII membranes with 0.5−1.5 mM $CuCl_2$ in a buffer containing 15 mM OGP, 0.4 M NaCl, 1 M sucrose, and 50 mM MES (pH 6) for 15 min leads to inhibition of the $O_2$-evolving activities to <10% of the original activity as shown in Table 3 and Figure 4. The reversibility of the treatment is examined by the addition of 20 mM $CaCl_2$. The deactivation of the PSII sample Cu1 is largely irreversible as only 18% of $O_2$-evolving activity is restored upon reconstitution of the Cu1 PSII sample with 20 mM $CaCl_2$. For the PSII samples Cu2 and Cu3, the $O_2$-evolving activity is partially restored to 58 and 67% of the original activity, respectively. The inhibitory effect of $CuCl_2$ on the $O_2$-evolving activity of PSII core complexes is

Table 2: Progressive Power Saturation of the $Y_D^{\bullet}$ Signal in Untreated PSII, $Dy^{3+}$-Inhibited PSII Core Complexes and $Dy^{3+}$-Inhibited PSII Membranes Measured on Varian EPR and Brüker EPR Spectrometers

| sample | untreated PSII | $Dy^{3+}$-PSII core complex | Dy7 | Dy4 | Dy1 |
|---|---|---|---|---|---|
| $Dy^{3+}$/PSII | 0 | 1 | 2 | 6 | 24 |
| $P_{1/2}$ measured on a Varian EPR spectrometer (raw data) | 0.27 wM ($R^2 = 0.9944$) | | 0.5 mW ($R^2 = 0.9986$) | 1.2 mW ($R^2 = 0.9921$) | 3.5 mW ($R^2 = 0.9967$) |
| $P_{1/2}$ measured on a Varian EPR spectrometer (normalized data)[a] | 0.034 mW | | 0.063 mW | 0.152 mW | 0.438 mW |
| $P_{1/2}$ measured on a Brüker EPR spectrometer | 0.034 mW ($R^2 = 0.9954$) | 0.066 mW ($R^2 = 0.9964$) | | | |
| $\Delta P_{1/2}$ | | 0.032 mW | 0 | 0.118 mW | 0.404 mW |
| distance ($Dy^{3+}$-$Y_D^{\bullet}$) | | 30 Å[b] | ≥40 Å[c] | 25 Å[c] | 20 Å[c] |

[a] The normalization factor is determined from the $P_{1/2}$ of the $S_2$ state multiline EPR signal of untreated PSII measured on both the Varian and Brüker EPR spectrometers. [b] Obtained from the X-ray crystal structure (*23*) assuming that $Dy^{3+}$ occupies the $Ca^{2+}$ site in the OEC. [c] Estimated by using $\Delta P_{1/2} \propto 1/r^6$ and assuming additive effects of one $Dy^{3+}$ bound to the $Ca^{2+}$ site in the OEC and a second $Dy^{3+}$ bound at a distance $r$ from $Y_D^{\bullet}$.

Table 3: Summary of the Characterization of $Cu^{2+}$-Inhibited PSII Samples

| $Cu^{2+}$-inhibited sample | % activity after $Cu^{2+}$ inhibition | $Cu^{2+}$ ions per PSII center | % activity after $Ca^{2+}$ reconstitution |
|---|---|---|---|
| Cu1[a] | $9 \pm 1$[d] | N/A | $18 \pm 3$[d] |
| Cu2[b] | $10 \pm 2$[e] | 11 | $58 \pm 1$[e] |
| Cu3[c] | $4 \pm 0$[f] | 8 | $67 \pm 4$[f] |
| $Cu^{2+}$-PSII core complex | $7 \pm 1$[g] | N/A | $17 \pm 1$[g] |

[a] Prepared from PSII membranes incubated with 1.5 mM $CuCl_2$. [b] Prepared from PSII membranes incubated with 0.5 mM $CuCl_2$. [c] Prepared from PSII membranes incubated with 0.5 mM $CuCl_2$ and Chelex 100 treated buffer. [d] Relative to activity of untreated PSII membranes at 488 $\mu$mol of $O_2$ (mg of Chl)$^{-1}$ h$^{-1}$. [e] Relative to activity of untreated PSII membranes at 403 $\mu$mol of $O_2$ (mg of Chl)$^{-1}$ h$^{-1}$. [f] Relative to activity of untreated PSII membranes at 362 $\mu$mol of $O_2$ (mg of Chl)$^{-1}$ h$^{-1}$. [g] Relative to activity of untreated PSII core complexes at 1228 $\mu$mol of $O_2$ (mg of Chl)$^{-1}$ h$^{-1}$.

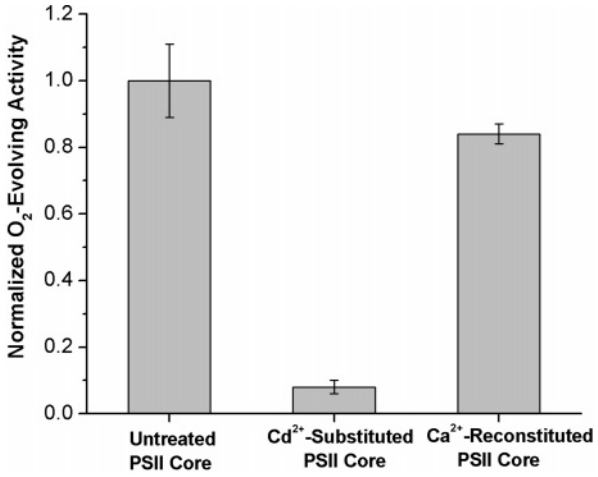


FIGURE 8: Comparison of the normalized $O_2$-evolving activity of untreated PSII core complexes, $Cd^{2+}$-inhibited PSII core complexes, and $Ca^{2+}$ reconstitution of $Cd^{2+}$-inhibited PSII core complexes. The oxygen-evolving activity of the treated PSII samples was normalized to the activity of untreated PSII at 1228 $\mu$mol of $O_2$ (mg of Chl)$^{-1}$ h$^{-1}$.

surveyed in the range of 0.05−2 mM $CuCl_2$. The addition of 2 mM $Cu^{2+}$ to PSII core complexes inhibits the $O_2$-evolving activity to 7% of the original activity, but reconstitution with excess $CaCl_2$ does not significantly restore the $O_2$-evolving activity, as shown in Table 3.

*(b) EPR Properties of $Cu^{2+}$-Inhibited PSII Membranes.* The EPR spectrum of $Cu^{2+}$-EDTA exhibits four hyperfine peaks at $g = 2.46$, $g = 2.34$, $g = 2.22$, and $g = 2.07$, with an average hyperfine splitting of ~ 171 G. The hyperfine peaks of the $Cu^{2+}$ ions ($g = 2.46$, 2.30, 2.17, and 2.08) in the PSII sample Cu2 and Cu3 are different from the EPR signals obtained from $Cu^{2+}$-EDTA. The average hyperfine coupling observed in the Cu3 PSII sample is ~163 G. The quantitation of $Cu^{2+}$ in PSII membranes was performed by comparison of the double integral of the $Cu^{2+}$ EPR signals at $g = 2.6$ to $g = 1.8$ in $Cu^{2+}$-inhibited PSII membranes to the $Cu^{2+}$ EPR signals in standard $Cu^{2+}$-EDTA samples. The results indicate that $Cu^{2+}$-inhibited PSII membrane samples have a large number of bound $Cu^{2+}$ ions; PSII samples Cu2 and Cu3 have 11 and 8 $Cu^{2+}$ ions per PSII center, respectively. $Cu^{2+}$-inhibited PSII membrane sample Cu3 was illuminated at 200 K for 5 min. The light-minus-dark spectrum of this sample displays an EPR signal growing in at $g = 2$, corresponding to the $Y_D^{\bullet}/Y_Z^{\bullet}$ EPR signals. However, the line shape of this light-induced EPR signal is quite different from the signal of $Y_D^{\bullet}$ in untreated PSII membranes (*42*), indicating that other radicals, such as chlorophyll and/or carotenoid radicals, are also formed. The $S_2$ state multiline EPR signal is not induced upon 200 K illumination for 5 min in $Cu^{2+}$-inhibited PSII membrane sample Cu3. Further, the $Q_A^{-}Fe^{2+}$ signal ($g = 1.82$ and 1.7 (*43*)) is also not observed in the Cu3 PSII sample.

*Inhibition by $Cd^{2+}$ Ions. (a) Oxygen-Evolution Inhibition Data.* The inhibition of oxygen evolution by $Cd^{2+}$ was conducted in PSII core complexes. As shown in Figure 4, the effects of incubation with 0.5 to 6 mM $CdCl_2$ were examined in this study. The treatment of PSII core complexes with 6 mM $CdCl_2$ yields 8% of the original $O_2$-evolving activity. Subsequent incubation of the PSII core samples with $CaCl_2$ restores the $O_2$-evolving activity to 84% (Figure 8) of the original activity of untreated PSII core complexes.

*(b) $S_1$ to $S_2$ State Transition in $Cd^{2+}$-Inhibited PSII.* The $S_1$ to $S_2$ state transition in $Cd^{2+}$-inhibited PSII is examined by illumination of the $Cd^{2+}$-inhibited PSII sample for 3 min under the same conditions used to induce the $S_2$ state multiline EPR signal in untreated PSII. As can be seen in Figure 9, $Cd^{2+}$-inhibited PSII exhibits an $S_2$ state multiline EPR signal upon illumination at 200 K that is very similar in both yield and line shape to the signal observed in untreated PSII core complexes. On the basis of the intensity of the $^{55}$Mn hyperfine peaks at $g = 2.33$ and $g = 2.25$ as marked in Figure 9, the yield of the $S_1$ to $S_2$ state transition

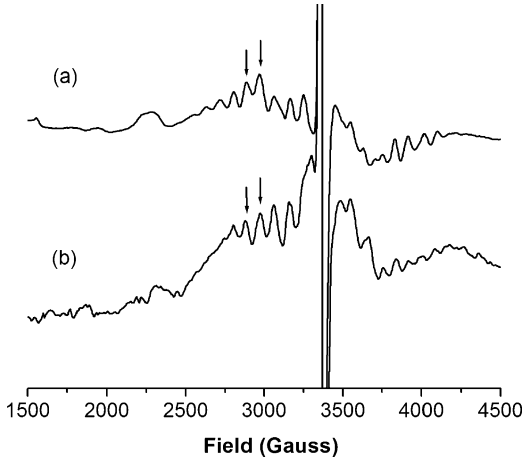


FIGURE 9: Comparison of the $S_2$ state multiline EPR signal induced by 200 K illumination for 3 min of (a) untreated PSII core complexes (3.9 mg of Chl/mL) and (b) $Cd^{2+}$-inhibited PSII core complexes (3.8 mg of Chl/mL). The EPR spectra were obtained from the light-minus dark difference of the individual spectra measured at 1 mW microwave power on a Brüker EPR spectrometer. The arrows indicate the $^{55}Mn$ hyperfine peaks associated with the $S_2$ multiline EPR signal, which were used for quantitation.

in $Cd^{2+}$-inhibited PSII core complexes is estimated to be 84% of the $S_1$ to $S_2$ state transition in untreated PSII core complexes.

## DISCUSSION

*Biochemistry and Quantitation of Metal−Ion Inhibition.* Cation treatments cause the loss of the $O_2$-evolving activity due to the replacement of $Ca^{2+}$, but they could also potentially disassemble the $Mn_4$ cluster of PSII (as is the case for the $Cu^{2+}$ treatment of PSII reported previously by Styring and co-workers (*44*)). Therefore, it is essential to examine the reversibility of the inhibition caused by the cation treatments by reconstitution of $Ca^{2+}$. In addition, previous studies have indicated that PSII membranes have several $Ca^{2+}$-binding sites, in addition to the $Ca^{2+}$-binding site in the OEC. To determine whether metal ions are bound to additional sites besides the $Ca^{2+}$-binding site in the OEC, we carefully quantitate the number of $Dy^{3+}$ and $Cu^{2+}$ per PSII based on their EPR signal intensity.

*Inhibition by Dy*$^{3+}$. $Dy^{3+}$ ion is a suitable EPR spin probe to replace $Ca^{2+}$ in PSII due to the similarity of the ionic radii of $Dy^{3+}$ and $Ca^{2+}$. Although $Dy^{3+}$ is a trivalent ion, previous studies have shown that it binds as a dipositive ion (*29*), presumably because $Dy^{3+}$ has a coordinated hydroxide. The EPR signal of $Dy^{3+}$ ($g \sim 16$) is distinct and does not overlap with the EPR signals arising from PSII components (*42*); therefore, the stoichiometry of $Dy^{3+}$ ions per PSII center can be quantified using the intensity of the $Dy^{3+}$ EPR signal. In addition, the spin−lattice relaxation rate of the $Dy^{3+}$ is rapid in comparison to the spin−lattice relaxation rate of the $Mn_4$ cluster and the $Y_D^{\bullet}$ radical of PSII. This difference in spin−lattice relaxation rates can be exploited to determine the location of $Dy^{3+}$ ions in PSII by monitoring the spin−lattice relaxation enhancement of the $Mn_4$ and $Y_D^{\bullet}$ EPR species in the presence of the $Dy^{3+}$ ions. Thus, the inhibition of oxygen evolution by $Dy^{3+}$ ions in the OEC can be utilized to determine both the location and function of the $Ca^{2+}$ cofactor in PSII. In contrast to previous studies (*34*, *45*), the $Dy^{3+}$-inhibited PSII samples in this study are prepared using an ion-exchange procedure in which $Ca^{2+}$ ions are not removed prior to the $Dy^{3+}$-inhibition of PSII (*29*, *30*). Thus, the PSII complexes remain structurally intact after the inhibitory treatments. This is confirmed by reconstitution of oxygen-evolution activity by addition of $Ca^{2+}$ to the $Dy^{3+}$-inhibited PSII. Further, $Dy^{3+}$ binding within the PSII core complex is confirmed by the effect of $Dy^{3+}$ ions on the EPR progressive power saturation behavior of the $S_2$ multiline and $Y_D^{\bullet}$ EPR signals.

As can be seen in Table 1, there is a loss of $O_2$-evolving activity of PSII complexes when $Dy^{3+}$ ions are added to PSII. The extent and reversibility of inhibition varies with the different treatments, with generally greater, and more irreversible, inhibition and more binding of $Dy^{3+}$ when higher concentrations of $DyCl_3$ are added.

Other than the $Ca^{2+}$-binding site in the OEC, two additional weak $Ca^{2+}$-binding sites in PSII have previously been reported in literature. One $Ca^{2+}$-binding site is suggested to be present on the CP29 polypeptide (*12*), and the second $Ca^{2+}$-binding site is suggested to be on the 33 kDa polypeptide of PSII (*7*, *8*). $Dy^{3+}$ ions can easily replace $Ca^{2+}$ in all three binding sites and could also bind to other metal-binding sites including nonspecific surface binding sites on the membranes. A study on the phosphorylation of the light-harvesting complexes has shown that, as the PSII membranes stack, two LHCII complexes may bind one $Ca^{2+}$ ion after the LHCII proteins are phosphorylated (*46*). One PSII membrane sample has 200 chlorophylls, and approximately 150 chlorophylls are located in the LHCII. On the basis of the knowledge that each LHCII contains 15 chlorophylls (*47*), the number of the LHCII in PSII membranes can be estimated to be 10. After the LHCII complexes are phosphorylated, five $Ca^{2+}$ ions could bind to the LHCII of stacked PSII membranes. Including the $Ca^{2+}$ ion in the OEC and $Ca^{2+}$ bound to the LHCII, six $Ca^{2+}$ ions in total could bind to each PSII membrane complex. This prediction is consistent with the characterization of Dy3 and Dy4 PSII samples as they both contain six $Dy^{3+}$ ions per PSII center (Table 1).

PSII samples treated with 20 mM $DyCl_3$ bind 24 $Dy^{3+}$/PSII and the number decreases to 6 $Dy^{3+}$/PSII upon treatment with OGP and EDTA (Dy3). When PSII membranes are treated with $\leq$0.5 mM $DyCl_3$, such as samples Dy4−Dy7, the number of bound $Dy^{3+}$ ions per PSII complex further decreases to $\leq$6 $Dy^{3+}$/PSII. When the light-harvesting complexes and the 17 and 23 kDa proteins are partially dissociated from the PSII core by the addition of high salt (0.4 M NaCl), most of the bound $Dy^{3+}$ ions dissociate into the solution. When the NaCl-treated PSII membranes with partially dissociated light-harvesting complexes and 17, 23 kDa proteins (PSII samples Dy5, Dy6, and Dy7) are treated with 0.1 mM $DyCl_3$, each PSII center is determined to have 2−3 $Dy^{3+}$/PSII. This is consistent with studies by Grove et al. (*6*) and Kalosaka et al. (*4*), which have reported that 17 and 23 kDa-depleted PSII has 2.5 high-affinity $Ca^{2+}$-binding sites per PSII.

The $Ca^{2+}$ site in the OEC has been proposed to be the strongest $Ca^{2+}$-binding site in PSII, and it has previously been suggested that the $Ca^{2+}$ ion located in the 33 kDa extrinsic protein of PSII membranes can be easily replaced by $Dy^{3+}$ ions for spectroscopic studies (*7*). This may explain why the minimum number of $Dy^{3+}$ ions per PSII membrane

determined in this study is two rather than one.

Although several studies have reported multiple $Ca^{2+}$-binding sites in PSII, in general, it is believed that the OEC has only one $Ca^{2+}$-binding site. However, previous $Dy^{3+}$-inhibition conditions in PSII membranes did not successfully yield samples with one $Dy^{3+}$ ion bound per PSII. In the present study, for the first time, we demonstrate that it is possible to substitute one $Dy^{3+}$ ion per PSII by the use of PSII core complexes, which are depleted of the LHCII and the 17, 23 kDa extrinsic polypeptides. In the absence of the 17 and 23 kDa extrinsic polypeptides, weakly bound ions in the $Ca^{2+}$-binding site in the 33 kDa extrinsic protein will dissociate with buffer washes.

EPR spectroscopic studies of PSII samples that have been treated with lanthanide ions (such as $Dy^{3+}$, $La^{3+}$, $Lu^{3+}$, and $Pr^{3+}$) have previously been reported by Bakou et al. (*34*, *45*). On the basis of the loss of the $S_2$ state multiline EPR signals in lanthanide-treated PSII samples, it was suggested that the $S_1$ to $S_2$ state transition is blocked by these cation treatments (*34*, *45*). These studies also reported that the amplitude of the light-induced EPR signal from $Y_Z^{\bullet}$ varies with the treated lanthanide ions (*45*) and the line shape of the $Y_D^{\bullet}$ EPR signal is broadened due to a magnetic interaction with the treated $Dy^{3+}$ ions (*34*). However, the PSII samples used in the measurements of $Y_D^{\bullet}$ by Bakou et al. contained 14−15 $Dy^{3+}$ ions per PSII complex (*34*). PSII samples with more than one $Dy^{3+}$ ion per PSII could lead to misinterpretation of the effects of $Dy^{3+}$ on the OEC, especially if $Dy^{3+}$ ions bind in sites outside of the OEC of PSII.

EPR progressive power saturation is commonly used to determine the location of paramagnetic centers in proteins by the measurement of the spin−lattice relaxation effects caused by long-range (<40 Å) spin−spin interactions (*48*). Measurements of $P_{1/2}$ provide information on the distance ($r$) between fast- and slow-relaxing spins because the change of $P_{1/2}$ caused by the spin−spin interaction is proportional to $1/r^6$. $Dy^{3+}$ is a fast-relaxing species and, therefore, the binding of $Dy^{3+}$ to the $Ca^{2+}$-site of the OEC or other $Ca^{2+}$ sites of PSII can be easily identified by the change of the power saturation of the $Y_D^{\bullet}$ and $S_2$ state multiline EPR signals.

The progressive power saturation behavior of the dark-stable $Y_D^{\bullet}$ radical of PSII was examined in untreated and $Dy^{3+}$-treated PSII samples to determine the location of $Dy^{3+}$ ions bound to PSII. As can be seen in Figure 7, binding of excess $Dy^{3+}$ to PSII membranes (sample Dy1 with 24 $Dy^{3+}$/PSII) causes a 13-fold increase in the $P_{1/2}$ of $Y_D^{\bullet}$ relative to that of untreated PSII membranes, whereas the binding of 1 $Dy^{3+}$ to PSII core complexes causes only a 2-fold increase. These results indicate that the highest affinity site is quite distant from $Y_D^{\bullet}$, consistent with the highest affinity $Dy^{3+}$-binding site being the $Ca^{2+}$-binding site of the OEC, which is known to be located 30 Å from $Y_D^{\bullet}$ based on the X-ray structures. When a larger number of $Dy^{3+}$ ions are bound to PSII, there are additional $Dy^{3+}$ ions bound in closer proximity to $Y_D^{\bullet}$ in the D2 polypeptide of PSII. The 13-fold increase of $P_{1/2}$ of $Y_D^{\bullet}$ in PSII membranes with 24 $Dy^{3+}$/PSII can either be due to one $Dy^{3+}$ ion bound at a short distance from $Y_D^{\bullet}$ or several $Dy^{3+}$ ions bound at slightly longer distances from $Y_D^{\bullet}$. Assuming that $Dy^{3+}$ in PSII core complexes (1 $Dy^{3+}$/PSII) is bound in the OEC, we can use the distance between the $Ca^{2+}$ ion of the OEC and the $Y_D^{\bullet}$ radical determined by the X-ray crystal structure (30 Å) as a reference. With this reference, we can estimate that a second $Dy^{3+}$ ion would have to be bound at a distance of 20 Å from the $Y_D^{\bullet}$ radical to account for the change of $P_{1/2}$ by $Dy^{3+}$ inhibition in sample Dy1. Notably, the 20 Å distance between $Dy^{3+}$ and $Y_D^{\bullet}$ is estimated with the assumption that the change of the power saturation is contributed solely by the additive effects of two $Dy^{3+}$ ions: one bound in the OEC and the second $Dy^{3+}$ ion closest to $Y_D^{\bullet}$. Similarly, the closest $Dy^{3+}$ to the $Y_D^{\bullet}$ radical in sample Dy4 can be estimated to be 25 Å from the $Y_D^{\bullet}$ radical. In sample Dy7, which has 2 $Dy^{3+}$/PSII, $P_{1/2}$ of $Y_D^{\bullet}$ is same as $P_{1/2}$ of $Y_D^{\bullet}$ in PSII core complexes with 1 $Dy^{3+}$/PSII. The same value of $P_{1/2}$ in the two PSII samples suggests that the second $Dy^{3+}$ in the sample with 2 $Dy^{3+}$/PSII is located ≥40 Å from $Y_D^{\bullet}$.

The PSII protein surfaces on the lumenal and stromal sides of the membrane are at distances of ∼27 and 26 Å, respectively, from $Y_D^{\bullet}$ according to an EPR study of PSII membranes depleted of all three extrinsic proteins (*49*). This EPR study on untreated PSII membranes also indicated that the distance from $Y_D^{\bullet}$ to the lumenal surface in the presence of the extrinsic proteins is ∼41 Å. According to these EPR distance measurements, surface bound $Dy^{3+}$ ions, on either the lumenal or the stromal side of the membrane, can affect the power saturation of $Y_D^{\bullet}$ in the absence of the extrinsic proteins. In terms of the power saturation effect on $Y_D^{\bullet}$, PSII core complexes are similar to extrinsic protein-depleted PSII membranes because the 17 and 23 kDa extrinsic proteins are removed. For sample Dy1, which retains the extrinsic proteins, the surface bound $Dy^{3+}$ ions on the lumenal side would be too distant to have a significant influence on the power saturation of $Y_D^{\bullet}$, while $Dy^{3+}$ ions in the stromal side could affect the power saturation of $Y_D^{\bullet}$. We searched for acidic residues as possible ligands of $Dy^{3+}$ ions within a radius of 19−21 Å of $Y_D^{\bullet}$ in the 3.5 Å X-ray crystal structure of PSII (*23*). No acidic residues were found at 19−21 Å from $Y_D^{\bullet}$ in the PSII structure. Therefore, we propose that the $Dy^{3+}$-binding site nearest to $Y_D^{\bullet}$ is not located in the PSII core. The structure of the PSII−LHCII supercomplex obtained by cryo-electron microscopy identified that light-harvesting proteins, the LHCII, CP29 and CP26, are attached to the CP43 and CP47 polypeptides of the PSII core (*50*). The distance between CP29 and $Y_D^{\bullet}$ is not known, but the closest $Dy^{3+}$-binding site to $Y_D^{\bullet}$ most likely is located on CP29 because the CP29 polypeptide is closer to $Y_D^{\bullet}$ than the CP26 polypeptide. Furthermore, a $Ca^{2+}$ site on CP29 has been previously reported (*12*).

PSII core complexes containing a single $Dy^{3+}$ ion exhibit the $S_2$ state multiline EPR signal upon low-temperature illumination. As can be seen in Figure 5, the $S_2$ state multiline EPR signal in $Dy^{3+}$-inhibited PSII core complexes is very similar to the $S_2$ state multiline EPR signal in untreated PSII, in contrast to the altered $S_2$ state multiline EPR signal observed in $Sr^{2+}$-inhibited PSII (*31*). However, $Dy^{3+}$ inhibition of PSII does lead to a slight broadening of the hyperfine peaks in comparison to those in untreated PSII. The X-ray crystal structure has characterized the distance of Ca−Mn as 3.3 and 4.0 Å (*23*). It might be expected that binding of $Dy^{3+}$ to the OEC in place of $Ca^{2+}$ would perturb the exchange interactions between the Mn ions and the electron−nuclear hyperfine interactions between the $S = 1/2$ spin of the $Mn_4$ cluster and the four $I = 5/2$ $^{55}Mn$ spins and, thereby,

alter the $S_2$ state multiline signal. There are two effects of $Dy^{3+}$ binding that need to be considered: the effect of the size and charge of $Dy^{3+}$ relative to $Ca^{2+}$ and the effect of the paramagnetism of $Dy^{3+}$.

Vrettos et al. (*29*) have shown that the $Ca^{2+}$ site in the OEC is a rigid, size-selective site. On the basis of this, we expect that $Dy^{3+}$ (and also $Cd^{2+}$) substitute into the $Ca^{2+}$ site better than $Sr^{2+}$ because they have much closer ionic radii (ionic radii of aqua $Ca^{2+}$, $Cd^{2+}$, $Dy^{3+}$, and $Sr^{2+}$ are 0.99, 0.97, 0.91, and 1.12 Å, respectively). Therefore, the perturbation of the $Mn_4$ geometry caused by $Dy^{3+}$ (or $Cd^{2+}$) substitution is expected to be smaller than that caused by $Sr^{2+}$; $Sr^{2+}$ is the only cation in this group that is too big to fit into the site. Note that Vrettos et al. (*29*) also have shown that $Ca^{2+}$, $Cd^{2+}$, $Sr^{2+}$, and $Dy^{3+}$ all bind as dipositive ions in the OEC, presumably because $Dy^{3+}$ has a coordinated hydroxide. Thus, there are no charge effects on the structure upon substitution of $Ca^{2+}$ by $Dy^{3+}$.

The spin−lattice relaxation rate of $Dy^{3+}$ has been estimated to be 6 ns at 6 K (*51*), which is much faster than the spin−lattice relaxation rate of $Mn_4$ cluster in the $S_2$ state at the same temperature (8 $\mu$s at 6 K, (*52*)). Thus, it is possible that the rapid spin−lattice relaxation rate of the $Dy^{3+}$ ion could average the exchange and dipolar interactions between the $Dy^{3+}$ spin and the $S_2$ state, which would render the line shape of the $S_2$ state multiline EPR signal in the $Dy^{3+}$-inhibited PSII core complexes very similar to the $S_2$ state multiline EPR signal in untreated PSII. For example, the broad low-temperature $S_2Y_Z^{\bullet}$ EPR signal of acetate-treated PSII converts to a narrow $Y_Z^{\bullet}$ EPR signal at room-temperature due to averaging of the exchange and dipolar interactions between $Y_Z^{\bullet}$ and the $S_2$ state of the $Mn_4$ cluster by rapid spin−lattice relaxation of the $Mn_4$ cluster (*53*).

We examine the effects of $Dy^{3+}$ inhibition on the progressive power saturation behavior of the $S_2$ state of the $Mn_4$ cluster to study the location of $Dy^{3+}$ in the $Dy^{3+}$-inhibited PSII samples. As shown in Figure 6, $P_{1/2}$ of the $S_2$ state multiline in $Dy^{3+}$-inhibited PSII core complexes containing a single $Dy^{3+}$ is 11-fold higher than $P_{1/2}$ of the $S_2$ state multiline in untreated PSII (9.9 and 0.92 mW, respectively). The enhancement of the $P_{1/2}$ value of the $S_2$ state multiline EPR signal upon $Dy^{3+}$ inhibition is due to the spin−spin interaction between the fast-relaxing $Dy^{3+}$ spin and the relatively slow-relaxing $Mn_4$ cluster.

We also observe that $Dy^{3+}$-inhibited PSII cores have only 7% of the original $O_2$-evolving activity of untreated PSII cores. This confirms that the $Dy^{3+}$ inhibition is nearly complete (∼93%) in PSII core complexes. We ascribe the residual activity to centers in which $Dy^{3+}$ has not replaced $Ca^{2+}$. Further, 62% of the original $O_2$-evolving activity of $Dy^{3+}$-inhibited PSII cores can be restored upon addition of excess $CaCl_2$. This indicates that the $Dy^{3+}$ treatment may have denatured the OEC in 38% of the PSII centers such that only 62% reconstitution of $O_2$-evolving activity is possible. The intensity of the $S_2$ state multiline EPR signals of $Dy^{3+}$-inhibited PSII is 24% of the intensity of the $S_2$ state multiline EPR signals in untreated PSII. This 24% yield of the $S_2$ state multiline signal in $Dy^{3+}$-inhibited PSII is low but still significantly more than the residual $Ca^{2+}$-bound PSII could form. The low yield of the $S_2$ state multiline EPR signal could be due to several reasons. First, the $S_1$ to $S_2$ state transition could be slowed down by $Dy^{3+}$ inhibition such that a complete reaction requires illumination at higher temperature, as has been observed in the case of low-pH treated PSII (*54*, *55*). In low-pH-treated PSII, the $S_2$ state multiline EPR signal is observed after illumination at 0 °C (70 °C higher than the illumination temperature to induce the normal $S_2$ multiline EPR signal). Second, there are 1−2 weak $Ca^{2+}$-binding sites in PSII besides the $Ca^{2+}$ in the OEC (*4*, *6*) that may affect the OEC (*10*, *11*). Ono and Inoue have investigated the effects of replacement of $Ca^{2+}$ by several divalent cations ($Cd^{2+}$, $Sr^{2+}$, $Mg^{2+}$, and $Ba^{2+}$) in PSII membranes after the depletion of $Ca^{2+}$ by a low-pH treatment (*11*). It was found that $Sr^{2+}$ and $Cd^{2+}$ ions have smaller effects on the thermoluminescence properties of the $S_2Q_A^-$ state than other divalent metal ions that were tested. It was suggested that one weakly bound $Ca^{2+}$ ion is essential for the $S_2$ to $S_3$ state transition. Kimura and Ono have studied the effect on carboxylate ligands in the OEC of depletion of weakly bound $Ca^{2+}$ ion(s) by high salt treatment (*56*). The FTIR spectra of these samples suggested that one $Ca^{2+}$ ion is close to the OEC, but not directly incorporated in the OEC. Kruk and co-workers proposed that a $Ca^{2+}$ ion on the 33 kDa extrinsic protein regulates the $H^+$ transfer through the water channel of the OEC (*7*). Recently, Barber and co-workers reinvestigated previous anomalous diffraction data (*23*) and have identified a $Ca^{2+}$ ion that binds to the 33 kDa protein at the exit of the putative proton channel (*8*). The distances between this bound $Ca^{2+}$ to $Y_D^{\bullet}$ and to the OEC are ∼60 Å and ∼35 Å, respectively (*8*). It is possible that a $Dy^{3+}$ ion binds to this $Ca^{2+}$ site; however, a $Dy^{3+}$ ion that binds to this $Ca^{2+}$ site is not expected to affect the power saturation behavior of the $S_2$ state multiline EPR signal significantly, contrary to the 11-fold increase of $P_{1/2}$ of the $S_2$ state multiline EPR signal observed in this study. Moreover, the $Dy^{3+}$-inhibited PSII core complexes studied here have only 1 $Dy^{3+}$/PSII on an average, such that most PSII centers should have $Dy^{3+}$ bound only to the high-affinity site in the OEC. It is conceivable that some PSII centers have $Dy^{3+}$ bound to another site that affects the activity of the OEC. In this case, somewhat more than 7% of the PSII centers could still have $Ca^{2+}$ bound in the OEC, if these centers do not evolve $O_2$ due to an inhibitory effect of $Dy^{3+}$ bound to another site. It seems unlikely, however, that the $Dy^{3+}$-inhibited PSII core complexes could have a sufficient fraction of active centers to account for the observation that 24% of $Dy^{3+}$-treated PSII core complexes (∼40% of PSII with reversibility) advance to the $S_2$ state. Moreover, such a second binding site would have to be very close to the $Mn_4$ cluster, so that binding of $Dy^{3+}$ to this site could significantly change the power saturation of the $S_2$ state multiline EPR signal.

Previous studies have concluded that $Ca^{2+}$-depleted PSII is capable of advancing to the $S_2$ state, but it has been reported that $Dy^{3+}$- (*34*, *35*), $La^{3+}$- (*35*), or $Cd^{2+}$-inhibited (*11*, *36*) PSII samples do not advance to the $S_2$ state upon illumination. To maintain the $S_n$ state transitions of PSII, it is important to preserve the intact structure of the OEC during the treatments to substitute other metal ions into the $Ca^{2+}$ site. In the study of Bakou et al. (*34*), the lanthanide treatments were irreversible, except for the sample of $Dy^{3+}$/EDTA-incubated PSII membranes. In the $Dy^{3+}$/EDTA-treated PSII membranes, $Ca^{2+}$ reconstitution recovered 43% of the original activity and the $Ca^{2+}$-reconstituted PSII

formed the $S_2$ state multiline EPR signal. However, this $Dy^{3+}$/EDTA-treated PSII sample did not form the $S_2$ state multiline EPR signal prior to the addition of $Ca^{2+}$ under the same sample illumination and spectrometer instrumental conditions used. In the present study, careful and systematic characterization of $Dy^{3+}$-inhibited PSII membranes (samples Dy1−Dy3) indicates that excess $Dy^{3+}$ can easily inhibit $O_2$-evolving activity but $Ca^{2+}$ reconstitution cannot restore the oxygen-evolving activity in these samples. We propose that the lack of $S_n$ state transitions in previous studies (*34*) could be due to alteration of the intact OEC structure with lanthanide treatment. If the same percentage of reconstitutable $Dy^{3+}$-inhibited PSII centers advance to the $S_2$ state as observed in the present study, then a $Dy^{3+}$-treated PSII membrane sample with 43% reversibility, as in the study of Bakou et al. (*34*), would be estimated to exhibit 17% of the $S_2$ state multiline EPR signal relative to untreated PSII. It is possible that it was not possible to detect such a low yield in the previous study considering that the $Dy^{3+}$/EDTA treated PSII membrane sample used by Bakou et al. was less concentrated (5 mg of Chl/mL) than the $Dy^{3+}$-inhibited PSII core complexes used in the present EPR measurements (3.1 mg of Chl/mL, equivalent to 15.5 mg of Chl/mL of PSII membranes).

*Inhibition by $Cu^{2+}$ and $Cd^{2+}$.* A comparison of the effects of divalent cations with those of $Dy^{3+}$ ions will help clarify the role of $Ca^{2+}$ ions in oxygen evolution. Brudvig and co-workers previously proposed that $Ca^{2+}$ functions in the OEC as a weak Lewis acid (*26*). $Cd^{2+}$ is ideal to replace $Ca^{2+}$ as it has a similar ionic radius (0.99 and 0.97 Å for $Ca^{2+}$ and $Cd^{2+}$, respectively, (*57*)) but is a stronger Lewis acid than $Ca^{2+}$ ($pK_a$'s of aqua $Cd^{2+}$ and $Ca^{2+}$ ions are 12.80 and 9.00, respectively (*58*)). In a prior study, $Cu^{2+}$ was found to inhibit oxygen evolution, although reversibility was not achieved (*44*). Studying the inhibition of oxygen evolution by $Cu^{2+}$ ions by using samples prepared with the same procedure used for $Dy^{3+}$-treated PSII provides more insight on the effect of $Cu^{2+}$ on the electron-transfer pathway.

$Cu^{2+}$ significantly inactivates the OEC (Table 3). For $Cu^{2+}$-inhibited PSII membrane samples, addition of excess $CaCl_2$ partially restores the $O_2$-evolving activity. The reversibility of inhibition is as high as 67 and 58% for samples Cu2 and Cu3, respectively. In PSII core complexes, the $O_2$-evolving activity is inhibited to 7% of the original activity by the addition of 2 mM $CuCl_2$, but the inhibition is not reversible. The inhibition of oxygen evolution caused by $Cu^{2+}$ treatment is conceivably a $Ca^{2+}$-dependent effect, although samples Cu2 and Cu3 are characterized to have 8 and 11 $Cu^{2+}$ ions per PSII center, respectively, which are more than the number of $Ca^{2+}$ ions in the PSII membrane samples. The hyperfine coupling of $Cu^{2+}$ ions in $Cu^{2+}$-inhibited PSII sample Cu3 is different from the hyperfine couplings in the EPR signal of aqueous $Cu^{2+}$-EDTA, which indicates that most of the added $Cu^{2+}$ ions are bound to PSII. The large number of $Cu^{2+}$ ions that bind to PSII indicates that PSII membranes have many unidentified binding sites for $Cu^{2+}$. The large extent of reversibility of $Cu^{2+}$-inhibited PSII membrane samples Cu2 and Cu3 indicates that the $Cu^{2+}$ treatment does not cause significant damage to the $Mn_4$ clusters in PSII membranes. The lack of reversibility for PSII core complexes might reflect the instability of the protein or inhibition that is not related to $Ca^{2+}$ in the OEC.

$Cd^{2+}$ ions are almost the same size as $Ca^{2+}$ ions and are, therefore, likely to bind well to $Ca^{2+}$ sites that discriminate metal ions by size. With the same charge as $Ca^{2+}$ ions, $Cd^{2+}$ ions will largely retain the charge distribution of the $Mn_4$ cluster. We find reversible inhibition of oxygen evolution by $Cd^{2+}$. Treatment of PSII core complexes with $Cd^{2+}$ inhibits the $O_2$-evolving activity to 8% of the original activity and the addition of excess $CaCl_2$ reactivates 84% of the $O_2$-evolving activity (Figure 8). The number of bound $Cd^{2+}$ ions bound to PSII was not characterized because $Cd^{2+}$ ions are EPR silent. Ono and Inoue (*11*) and Sigfridsson et al. (*37*) have studied the interaction of $Cd^{2+}$ with PSII, including the effects on the electron donor and acceptor sides, and the inhibition of $O_2$ evolution by a $Ca^{2+}$-dependent reaction. The reversibility of $Cd^{2+}$ inhibition is a key difference for the $Cd^{2+}$-inhibited PSII core complexes used in the present investigation and these previous studies.

As shown in Figure 9, an $S_2$ state multiline EPR signal is observed in $Cd^{2+}$-inhibited PSII core complexes, and this signal is very similar to that in untreated PSII. From the good correlation between the extent of reversibility of $Cd^{2+}$ treatment and the yield of the $S_2$ state multiline EPR signal in $Cd^{2+}$-inhibited PSII core complexes (both 84%), it is clear that $Cd^{2+}$-inhibited PSII centers are capable of advancing from the $S_1$ to the $S_2$ state. Because $Cd^{2+}$ is diamagnetic, the binding of $Cd^{2+}$ to the OEC would only affect the line shape of the $S_2$ state multiline signal if $Cd^{2+}$ ions change the geometry of the $Mn_4$ cluster. The observation of very similar $S_2$ state multiline EPR signals in both $Cd^{2+}$-inhibited and untreated PSII core complexes indicates that $Cd^{2+}$ binds to the calcium site in the OEC with very little structural perturbation, consistent with the similar ionic radii of $Ca^{2+}$ and $Cd^{2+}$.

*Role of $Ca^{2+}$ in the Oxygen-Evolution Reaction.* In the models proposed by Brudvig, Pecoraro, and co-workers, $Ca^{2+}$ is suggested to function as a Lewis acid that binds and activates a substrate water molecule (or hydroxide ion) for nucleophilic attack on a Mn(V)═O species in the O−O bond-formation reaction (*26*, *28*). The OEC remains active when $Ca^{2+}$ is replaced by $Sr^{2+}$, although the activity is reduced to ∼40% of untreated PSII. This functional replacement of $Ca^{2+}$ by $Sr^{2+}$ has been ascribed to the similar $pK_a$ of $Ca^{2+}$ and $Sr^{2+}$ ions (*26*, *29*). Notably, the substitution of $Ca^{2+}$ by $Sr^{2+}$ changes the $pK$a of the protonation reaction in the OEC (*30*). The upshift of the $pK$a by $Sr^{2+}$ substitution supports the proposal that $Ca^{2+}$ acts as a Lewis acid in the oxygen-evolution reaction.

$Dy^{3+}$ and $Cd^{2+}$ inhibition of the OEC cause the loss of $O_2$-evolving activity, but this work shows that both $Dy^{3+}$- and $Cd^{2+}$-inhibited PSII core complexes are capable of advancing from the $S_1$ to the $S_2$ state. These observations are consistent with the previous observation that $Ca^{2+}$-depleted PSII forms the $S_2$ state multiline EPR signal upon illumination at 200 K and indicate that the specific functional role of $Ca^{2+}$ in the OEC is beyond the $S_2$ state, as proposed by Brudvig, Pecoraro, and co-workers.

## CONCLUSIONS

In conclusion, we present a new, reversible procedure to substitute metal ions into the calcium-binding site in the OEC and provide quantitation of the substituted metal ions and

distance estimates for the locations of bound metal ions. The observation that both $Dy^{3+}$- and $Cd^{2+}$-inhibited PSII core complexes that are capable of advancing from the $S_1$ to the $S_2$ state provides support for the proposal that $Ca^{2+}$ plays a structural role in the early S state transitions, which can be fulfilled by other cations of similar ionic radius, and that the functional role of $Ca^{2+}$ to activate water in the O−O bond-forming reaction, which occurs in the final step of the S state cycle, can only be fulfilled by $Ca^{2+}$ and $Sr^{2+}$, two cations with similar Lewis acidities. As $Ca^{2+}$ is a spectroscopically silent ion, there has long been a quest for more informative metal ions to be substituted into the $Ca^{2+}$-binding site of PSII. This work successfully introduces a new method for further studies to understand oxygen evolution in PSII.

## REFERENCES


1. Debus, R. J. (1992) The manganese and calcium ions of photosynthetic oxygen evolution, *Biochim. Biophys. Acta 1102*, 269−352.
2. McEvoy, J. P., and Brudvig, G. W. (2006) Water-splitting chemistry of photosystem II, *Chem. Rev. 106*, 4455−4483.
3. Han, K. C., and Katoh, S. (1995) Different binding affinity sites of $Ca^{2+}$ for reactivation of oxygen evolution in NaCl-washed photosystem II membranes represent differently modified states of a single binding site, *Biochim. Biophys. Acta 1232*, 230−236.
4. Kalosaka, K., Beck, W. F., Brudvig, G. W., and Cheniae, G. (1990) Coupling of the PS2 reaction center to the oxygen-evolving center requires a very high affinity $Ca^{2+}$ site, in *Current Research in Photosynthesis* (Baltscheffsky, M., Ed.), pp 721−724, Kluwer Academic Publishers, Dordrecht, The Netherlands.
5. Adelroth, P., Lindberg, K., and Andreasson, L. E. (1995) Studies of $Ca^{2+}$ binding in spinach photosystem II using $^{45}Ca^{2+}$, *Biochemistry 34*, 9021−9027.
6. Grove, G. N., and Brudvig, G. W. (1998) Calcium binding studies of photosystem II using a calcium-selective electrode, *Biochemistry 37*, 1532−1539.
7. Kruk, J., Burda, K., Jemiola-Rzeminska, M., and Strzalka, K. (2003) The 33 kDa protein of photosystem II is a low-affinity calcium- and lanthanide-binding protein, *Biochemistry 42*, 14862−14867.
8. Murray, J. W., and Barber, J. (2006) Identification of a calcium-binding site in the PsbO protein of photosystem II, *Biochemistry 45*, 4128−4130.
9. Jegerschold, C., MacMillan, F., Lubitz, W., and Rutherford, A. W. (1999) Effects of copper and zinc ions on photosystem II studied by EPR spectroscopy, *Biochemistry 38*, 12439−12445.
10. Shen, J.-R., Satoh, K., and Katoh, S. (1988) Calcium content of oxygen-evolving photosystem II preparations from higher plants: effects of NaCl treatment, *Biochim. Biophys. Acta 933*, 358−364.
11. Ono, T. A., and Inoue, Y. (1989) Roles of $Ca^{2+}$ in $O_2$ evolution in higher plant photosystem II: Effects of replacement of $Ca^{2+}$ site by other cations, *Arch. Biochem. Biophys. 275*, 440−448.
12. Jegerschold, C., Rutherford, A. W., Mattioli, T. A., Crimi, M., and Bassi, R. (2000) Calcium binding to the photosystem II subunit CP29, *J. Biol. Chem. 275*, 12781−12788.
13. Boussac, A., Rappaport, F., Carrier, P., Verbavatz, J. M., Gobin, R., Kirilovsky, D., Rutherford, A. W., and Sugiura, M. (2004) Biosynthetic $Ca^{2+}/Sr^{2+}$ exchange in the photosystem II oxygen-evolving enzyme of *Thermosynechococcus elongatus*, *J. Biol. Chem. 279*, 22809−22819.
14. Suzuki, H., Taguchi, Y., Sugiura, M., Boussac, A., and Noguchi, T. (2006) Structural perturbation of the carboxylate ligands to the manganese cluster upon $Ca^{2+}/Sr^{2+}$ exchange in the S-state cycle of photosynthetic oxygen evolution as studied by flash-induced FTIR difference spectroscopy, *Biochemistry 45*, 13454−13464.
15. Barry, B. A., Hicks, C., De Riso, A., and Jenson, D. L. (2005) Calcium ligation in photosystem II under inhibiting conditions, *Biophys. J. 89*, 393−401.
16. De Riso, A., Jenson, D. L., and Barry, B. A. (2006) Calcium exchange and structural changes during the photosynthetic oxygen evolving cycle, *Biophys. J. 91*, 1999−2008.
17. Latimer, M. J., DeRose, V. J., Mukerji, I., Yachandra, V. K., Sauer, K., and Klein, M. P. (1995) Evidence for the proximity of calcium to the manganese cluster of photosystem II: Determination by X-ray absorption spectroscopy, *Biochemistry 34*, 10898−10909.
18. Cinco, R. M., Robblee, J. H., Rompel, A., Fernandez, C., Yachandra, V. K., Sauer, K., and Klein, M. P. (1998) Strontium EXAFS reveals the proximity of calcium to the manganese cluster of oxygen-evolving photosystem II, *J. Phys. Chem. B 102*, 8248−8256.
19. Latimer, M. J., DeRose, V. J., Yachandra, V. K., Sauer, K., and Klein, M. P. (1998) Structural effects of calcium depletion on the manganese cluster of photosystem II: Determination by X-ray absorption spectroscopy, *J. Phys. Chem. B 102*, 8257−8265.
20. Penner-Hahn, J. E., Fronko, R. M., Pecoraro, V. L., Yocum, C. F., Betts, S. D., and Bowlby, N. R. (1990) Structural characterization of the manganese sites in the photosynthetic oxygen-evolving complex using X-ray absorption spectroscopy, *J. Am. Chem. Soc. 112*, 2549−2557.
21. Zouni, A., Witt, H. T., Kern, J., Fromme, P., Krauss, N., Saenger, W., and Orth, P. (2001) Crystal structure of photosystem II from *Synechococcus elongatus* at 3.8 angstrom resolution, *Nature 409*, 739−743.
22. Kamiya, N., and Shen, J. R. (2003) Crystal structure of oxygen-evolving photosystem II from *Thermosynechococcus vulcanus* at 3.7 angstrom resolution, *Proc. Natl. Acad. Sci. U.S.A. 100*, 98−103.
23. Ferreira, K. N., Iverson, T. M., Maghlaoui, K., Barber, J., and Iwata, S. (2004) Architecture of the photosynthetic oxygen-evolving center, *Science 303*, 1831−1838.
24. Loll, B., Kern, J., Saenger, W., Zouni, A., and Biesiadka, J. (2005) Towards complete cofactor arrangement in the 3.0 angstrom resolution structure of photosystem II, *Nature 438*, 1040−1044.
25. Hoganson, C. W., and Babcock, G. T. (1997) A metalloradical mechanism for the generation of oxygen from water in photosynthesis, *Science 277*, 1953−1956.
26. Vrettos, J. S., Limburg, J., and Brudvig, G. W. (2001) Mechanism of photosynthetic water oxidation: Combining biophysical studies of photosystem II with inorganic model chemistry, *Biochim. Biophys. Acta 1503*, 229−245.
27. Siegbahn, P. E. M., and Crabtree, R. H. (1999) Manganese oxyl radical intermediates and O−O bond formation in photosynthetic oxygen evolution and a proposed role for the calcium cofactor in photosystem II, *J. Am. Chem. Soc. 121*, 117−127.
28. Pecoraro, V. L., Baldwin, M. J., Caudle, M. T., Hsieh, W.-Y., and Law, N. A. (1998) A proposal for water oxidation in photosystem II, *Pure Appl. Chem. 70*, 925−929.
29. Vrettos, J. S., Stone, D. A., and Brudvig, G. W. (2001) Quantifying the ion selectivity of the $Ca^{2+}$ site in photosystem II: Evidence for direct involvement of $Ca^{2+}$ in $O_2$ formation, *Biochemistry 40*, 7937−7945.
30. Lee, C.-I., and Brudvig, G. W. (2004) Investigation of the functional role of $Ca^{2+}$ in the oxygen-evolving complex of photosystem II: A pH-dependence study of the substitution of $Ca^{2+}$ by $Sr^{2+}$, *J. Chin. Chem. Soc. 51*, 1221−1228.
31. Boussac, A., and Rutherford, A. W. (1988) Nature of the inhibition of the oxygen-evolving enzyme of photosystem II induced by NaCl washing and reversed by the addition of $Ca^{2+}$ or $Sr^{2+}$, *Biochemistry 27*, 3476−3483.
32. Boussac, A., Zimmermann, J.-L., and Rutherford, A. W. (1989) EPR signals from modified charge accumulation states of the oxygen evolving enzyme in $Ca^{2+}$-deficient photosystem II, *Biochemistry 28*, 8984−8989.
33. Lakshmi, K. V., Eaton, S. S., Eaton, G. R., Frank, H. A., and Brudvig, G. W. (1998) Analysis of dipolar and exchange interactions between manganese and tyrosine Z in the $S_2Y_Z^{\bullet}$ state of acetate-inhibited photosystem II via EPR spectral simulations at X- and Q-Bands, *J. Phys. Chem. B 102*, 8327−8335.
34. Bakou, A., Buser, C., Dandulakis, G., Brudvig, G., and Ghanotakis, D. F. (1992) Calcium-binding site (s) of photosystem II as probed by lanthanides, *Biochim. Biophys. Acta 1099*, 131−136.
35. Ono, T. (2000) Effect of lanthanide substitution at $Ca^{2+}$-site on the properties of the oxygen evolving center of photosystem II, *J. Inorg. Biochem 82*, 85−91.
36. Pagliano, C., Raviolo, M., Dalla Vecchia, F., Gabbrielli, R., Gonnelli, C., Rascio, N., Barbato, R., and La Rocca, N. (2006) Evidence for PSII donor-side damage and photoinhibition induced by cadmium treatment on rice (*Oryza sativa L.*), *J. Photochem. Photobiol. B-Biol. 84*, 70−78.
37. Sigfridsson, K. G. V., Bernat, G., Mamedov, F., and Styring, S. (2004) Molecular interference of $Cd^{2+}$ with photosystem II, *Biochim. Biophys. Acta 1659*, 19−31.

38. Berthold, D. A., Babcock, G. T., and Yocum, C. F. (1981) A highly resolved, oxygen-evolving photosystem II preparation from spinach thylakoid membranes: EPR and electron-transport properties, *FEBS Lett. 134*, 231−234.
39. Beck, W. F., de Paula, J. C., and Brudvig, G. W. (1985) Active and resting states of the $O_2$-evolving complex of photosystem II, *Biochemistry 24*, 3035−3043.
40. Ghanotakis, D. F., Demetriou, D. M., and Yocum, C. F. (1987) Isolation and characterization of an oxygen-evolving photosystem II reaction center core preparation and a 28 kDa Chl-*a*-binding protein, *Biochim. Biophys. Acta 891*, 15−21.
41. Aasa, R., and Vänngård, T. (1975) EPR signal intensity and powder shapes - Re-examination, *J. Magn. Res. 19*, 308−315.
42. Miller, A.-F., and Brudvig, G. W. (1991) A guide to electron paramagnetic resonance spectroscopy of photosystem II membranes, *Biochim. Biophys. Acta 1056*, 1−18.
43. Rutherford, A. W., and Zimmerman, J. -L. (1984) A new EPR signal attributed to the primary plastosemiquinone acceptor in photosystem II, *Biochim. Biophys. Acta 767*, 168−175.
44. Jegerschold, C., Arellano, J. B., Schroder, W. P., van Kan, P. J. M., Baron, M., and Styring, S. (1995) Copper(II) inhibition of electron transfer through photosystem II studied by EPR spectroscopy, *Biochemistry 34*, 12747−12754.
45. Bakou, A., and Ghanotakis, D. F. (1993) Substitution of lanthanides at the calcium site(s) in photosystem II affects electron transport from tyrosine Z to $P680^+$, *Biochim. Biophys. Acta 1141*, 303−308.
46. Stys, D. (1995) Stacking and separation of photosystem I and photosystem II in plant thylakoid membranes: A physico-chemical view, *Physiol. Plant. 95*, 651−657.
47. Kühlbrandt, W., and Wang, D. (1991) 3-dimensional structure of plant light-harvesting complex determined by electron crystallography, *Nature 350*, 130−134.
48. Lakshmi, K. V., and Brudvig, G. W. (2001) Pulsed electron paramagnetic resonance methods for macromolecular structure determination, *Curr. Opin. Struct. Biol. 11*, 523−531.
49. Innes, J. B., and Brudvig, G. W. (1989) Location and magnetic relaxation properties of the stable tyrosine radical in photosystem II, *Biochemistry 28*, 1116−1125.
50. Nield, J., Orlova, E. V., Morris, E. P., Gowen, B., van Heel, M., and Barber, J. (2000) 3D map of the plant photosystem II supercomplex obtained by cryoelectron microscopy and single particle analysis, *Nature Struct. Biol. 7*, 44−47.
51. Fish, G. E., North, M. H., and Stapleton, H. J. (1980) Test of orbit-lattice interaction models using spin-lattice relaxation data of $Er^{3+}$, $Dy^{3+}$, and $Yb^{3+}$ in $Cs_2NaYCl_6$, *J. Chem. Phys. 73*, 4807−4815.
52. Lorigan, G. A., and Britt, R. D. (2000) Electron spin-lattice relaxation studies of different forms of the $S_2$ state multiline EPR signal of the photosystem II oxygen-evolving complex, *Photosynth. Res. 66*, 189−198.
53. Szalai, V. A., Kühne, H., Lakshmi, K. V., and Brudvig, G. W. (1998) Characterization of the interaction between manganese and tyrosine Z in acetate-inhibited photosystem II, *Biochemistry 37*, 13594−13603.
54. Ono, T. A., and Inoue, Y. (1990) A marked upshift in threshold temperature for the $S_1$-to-$S_2$ transition induced by low pH treatment of PS II membranes, *Biochim. Biophys. Acta 1015*, 373−377.
55. Ono, T., Kusunoki, M., Matsushita, T.; Oyanagi, H., and Inoue, Y. (1991) Structural and functional modifications of the manganese cluster in $Ca^{2+}$-depeted $S_1$ and $S_2$ states: Electron paramagnetic resonance and X-ray absorption spectroscopy studies, *Biochemistry 30*, 6836−6841.
56. Kimura, Y., and Ono, T. (2001) Chelator-induced disappearance of carboxylate stretching vibrational modes in $S_2/S_1$ FTIR spectrum in oxygen-evolving complex of photosystem II, *Biochemistry 40*, 14061−14068.
57. Weast, R. C., Ed. (1978) *CRC Handbook of Chemistry and Physics*, CRC Press, Inc., West Palm Beach.
58. Dean, J. A. (1985) *Lange's Handbook of Chemistry*, McGraw-Hill Book Co., New York.

BI062033I